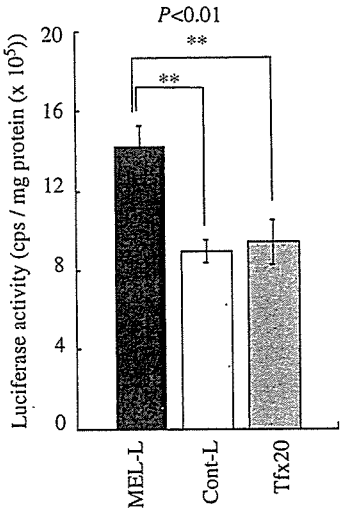

Fig. 2. Effect of MEL-A on transfection efficiency of MEL-L, Cont-L and Tfx20 in Hela cells. Lipoplexes were diluted in medium with serum to a final concentration of 2 μg of DNA in 1 ml of medium per well, and each cell was incubated for 24 h. The charge ratio (+/−) of liposome to plasmid DNA was 3:1. Each result represents the mean±S.D. (n=3).

Cont-L and Tfx20. This suggested that MEL-A enhanced the transfection efficiency of the DC-Chol/DOPE liposome. We also confirmed that MEL-L had no toxicity when the MEL-lipoplex was incubated with Hela cells at the dose used (data not shown). These results were consisted with the finding that cationic liposomes containing MEL-A promoted the efficiency of gene transfection into mammalian cultured cells although MEL-A itself did not increase transfection efficiency [15]. The effect on transfection efficiency might be because MEL-A minimized the aggregation induced by DNA and reduced particle size [10,17].

3.3. Localization of liposome and DNA transfected into Hela cells

To investigate the intracellular localization of the MEL-lipoplex, we prepared lipoplexes of either DiI-labeled MEL-L or Cont-L with FITC-ODN and transfected them into Hela cells (Fig. 3). After 2 or 24 h of incubation, the intracellular localization of the DiI-labeled liposome and FITC-labeled DNA were confirmed by changing the Z-axis of the observed area

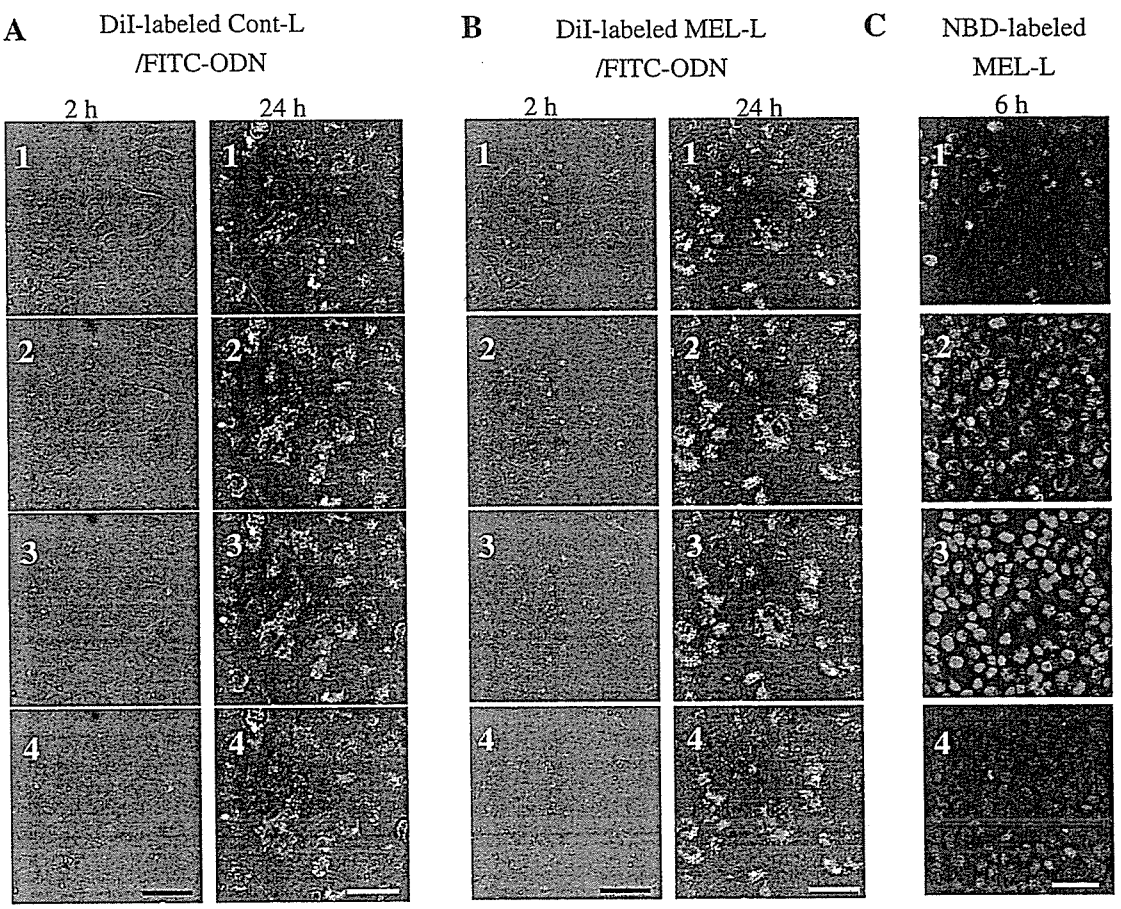

Fig. 3. The localization of lipoplexes of DiI-labeled liposome and FITC-ODN at 2 and 24 h after incubation (A and B). FITC-ODN was mixed with DiI-labeled Cont-L (A) and MEL-L (B), respectively. The localization of lipoplexes of MEL-L with NBD-labeled MEL-A and plasmid DNA at 6 h after incubation (C). Plasmid DNA was mixed with NBD-labeled MEL-L. The lipoplexes were transfected into Hela cells, and observed under a confocal laser microscope by changing the Z-axis. Images 1–4 represent regular intervals of 3 μm on the Z-axis from bottom to top of cells, respectively. In A and B, the red signals show the location of the liposome, and the green signals, that of the FITC-ODN. In C, the red signals show the location of the nucleus, and the green signals, that of the MEL-A. Scale bar=50 μm.

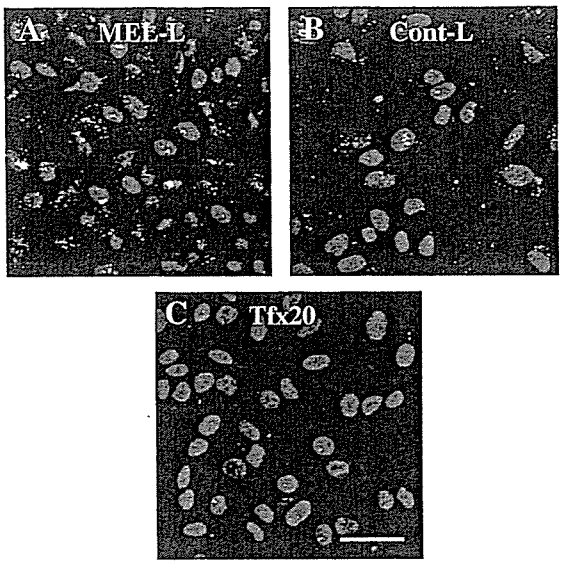

Fig. 4. Intracellular distribution of FITC-ODN by liposomes in Hela cells. FITC-ODN was transfected by MEL-L (A), Cont-L (B) and Tfx20 (C), respectively, into Hela cells. After 6 h of incubation, nuclei were stained by PI, and the cells were examined under a fluorescent microscope using a filter for green-fluorescence (FITC-ODN) and red-fluorescence (nucleus). Scale bar=50 μm.

with 3 μm. DiI-fluorescence was weakly detected in the cytoplasm at 2 h incubation with MEL-L (Fig. 3B), but hardly detected with Cont-L (Fig. 3A). This indicated that MEL-L was rapidly internalized into the cells. At 24 h, DiI-fluorescence and FITC-fluorescence in both MEL-L and Cont-L were widely observed in the cytoplasm.

To confirm the distribution of the DiI-fluorescence of MEL-L by MEL-A, we prepared lipoplexes using NBD-labeled MEL-L with NBD-labeled MEL-A and transfected them into Hela cells. After 6 h of incubation, NBD-labeled MEL-A was widely observed in the cytoplasm but not detected in the nucleus (Fig. 3C). This localization was similar to that of DiI-labeled MEL-L (Fig. 3B) and suggested that MEL-A of MEL-L enhanced the association of MEL-lipoplex with the cells and induced the distribution of liposome and DNA into the cytoplasm. This might explain the enhancement of transfection efficiency by MEL-A. Inoh et al. reported that lipoplexes containing MEL-A and OH-Chol were temporarily located on the plasma membrane of target cells [15]. However, our results showed that MEL-A was located throughout the cytoplasm. We cannot explain this discrepancy, but the difference in cationic lipids might affect the distribution of MEL-L in the target cell.

To confirm the localization of DNA in the cells, lipoplexes of FITC-ODN were formed with MEL-L, Cont-L and Tfx20, respectively, and transfected into Hela cells. The fluorescence of FITC-ODN in the cells was more strongly observed in MEL-L than in Cont-L at 6 h of incubation (Fig. 4A and B). In MEL-L, FITC-ODN was distributed around the nucleus and cytoplasm, but in Cont-L, it was mostly localized to the cytoplasm. In Tfx20, little fluorescence was observed (Fig. 4C). This suggested that MEL-L could deliver DNA into the cytoplasm and nucleus better than Cont-L or Tfx20.

3.4. Association of MEL-, Cont- and, Tfx20-lipoplexes with the cells

To compare the cellular association of the DNA transfected by MEL-L, Cont-L and Tfx20, respectively, we examined the

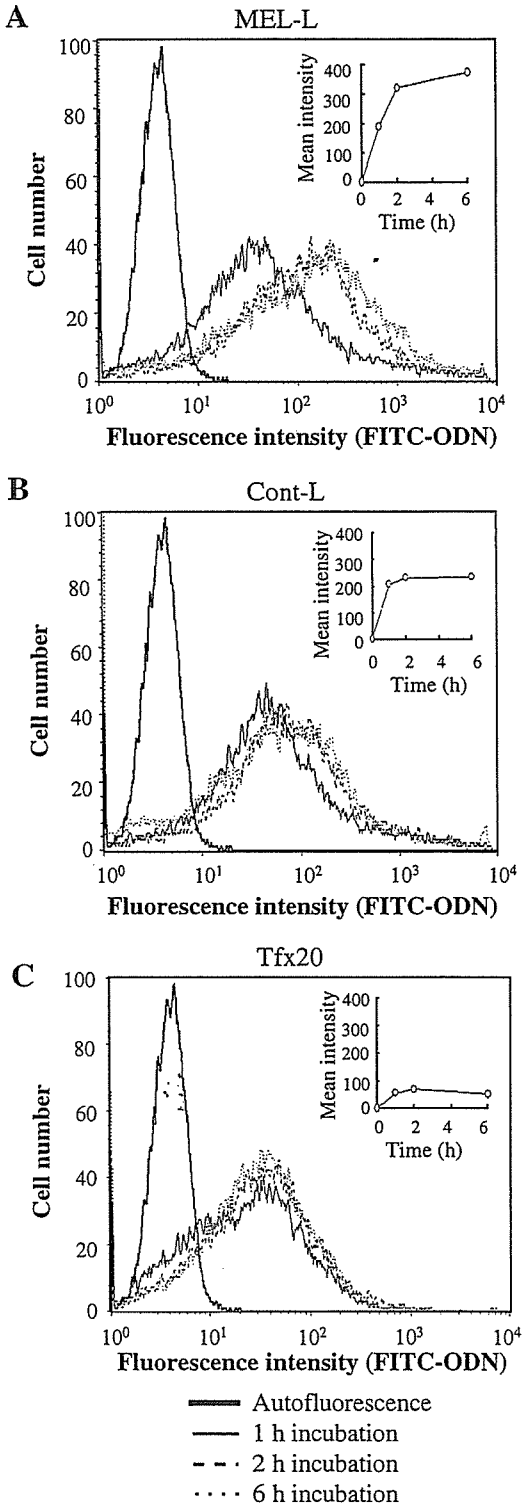

Fig. 5. The cellular association with lipoplexes of FITC-ODN. The kinetics of the cellular association of FITC-ODN transfected with MEL-L (A), Cont-L (B) and Tfx20 (C) was evaluated by flow cytometry. Each lipoplex was incubated with cells for 1, 2 and 6 h.

amount of DNA associated with the cells at different time points by flow cytometry. Analysis of flow cytometric profiles and mean intensities clearly indicated that the kinetics of the amount of DNA was remarkably different among MEL-L, Cont-L and Tfx20 (Fig. 5). The fluorescent intensity of FITC-ODN was stronger in MEL-L than in Cont-L (Fig. 5A and B). The fluorescence intensity of Cont-lipoplex increased rapidly, but reached a maximum at 1 h. In contrast, the fluorescence intensity of the MEL-lipoplex increased with time for up to 6 h. This might be corresponding with the observation of lipoplex using NBD-labeled MEL-L (Fig. 3C). The fluorescence intensity in Tfx20 was much weaker than these in MEL-L and Cont-L (Fig. 5C). The kinetics of the amount of DiI-labeled liposome was also similar with that of FITC-labeled DNA. After 24 h of incubation, the fluorescent intensity of the lipoplexes of DiI-labeled MEL-L was maintained whereas that of DiI-labeled Cont-L was decreased compared with that after 2 h of incubation (data not shown). These findings indicated that MEL-A enhanced and sustained the association of liposomes with cells.

The results of confocal laser microscopy and flow cytometry showed that MEL-A enhanced the interaction between lipoplexes and cells and quickly internalized lipoplexes and widely distributed them into the cytoplasm. MEL-A may have improved transfection activity by enhancing and sustaining the interaction between the lipoplexes and cells.

The entry into the cytoplasm is the first important step for liposome-mediated transfection. The addition of MEL-A to cationic liposomes with either DC-Chol or OH-Chol had a similar enhancing effect on transfection efficiency [15]. Confocal laser scanning microscopy revealed that MEL-A increased membrane fusion by liposomes with OH-Chol [15], but not that by liposomes with DC-Chol. In liposomes with OH-Chol, both MEL-A and DNA distributed on the plasma membrane, and DNA was internalized via fusion [15]. In MEL-L with DC-Chol, MEL-A and DNA distributed through the cytoplasm (Figs. 3 and 4), and the transfection activity was decreased by addition of endocytosis inhibitor, chloroquine (data not shown), suggesting that MEL-L was internalized into the cells via endocytosis. Our DC-Chol/DOPE liposomes were different from their DC-Chol/DOPE and OH-Chol/DOPE liposomes: in our case, the preparation involved a modified ethanol injection; the molar ratio of DC-Chol/DOPE was 3:2, the concentration of MEL-A in DC-Chol/DOPE liposomes was different, and the lipoplexes were formed by mixing the liposome with DNA directly in water without pre-incubation. In both cases, we can say that the addition of MEL-A to DC-Chol/DOPE liposomes decreased the size of the liposomes and lipoplexes, induced a rapid uptake of DNA in the cytoplasm, and increased transfection efficiency. However, the mechanism of enhancement by MEL-A was not similar with OH-Chol/DOPE liposomes [15], suggesting that cationic lipids also play an important role in facilitating the transfection. The role of DC-Chol in the formation of lipoplexes is presently unknown, but must be important in determining the final transfection efficiency.

MEL-L increased the association of lipoplexes with cell membranes, not by aggregation of lipoplexes. This better association results in better penetration by the lipoplexes. Biosurfactants of MEL-A have many excellent properties (low toxicity, biodegradability, etc.) compared to synthetic surfactants [18,19]. The combination of MEL-A and a cationic lipid might increase transfection efficiency via a synergetic effect. Furthermore, MEL-lipoplexes remained small in size and enhanced transfection efficiency in serum, which is important for applications in vivo. These findings suggested that MEL-L is a remarkable non-viral vector for gene transfection and gene therapy.

4. Conclusions

In the present study, we studied the transfection efficiency of MEL-L and investigated the localization and kinetics of lipoplexes to understand the mechanism of the enhancement of transfection efficiency by MEL-A. The transfection efficiency of MEL-L was significantly higher than that of Cont-L or Tfx20. We found that MEL-L increased the association with the cells in the experiment with flow cytometry, and the lipoplexes distributed widely in the cytoplasm and around the nucleus by confocal laser microscopy. These findings may be one of the reasons why MEL-L enhanced the transfection efficiency of MEL-A. These findings indicate that cationic liposomes containing MEL-A have potential as an effective vector in gene therapy.

Acknowledgements

We thank Dr. Kitamoto (National Institute of Advanced Industrial Science and Technology, Tsukuba, Japan) for supplying MEL-A. This project was supported in part by a grant from The Promotion and Mutual Aid Corporation for Private Schools of Japan, and by a Grant-in Aid for Scientific Research from the Ministry of Education, Culture, Sports, Science, and Technology of Japan.

References

[1] X. Gao, L. Huang, A novel cationic liposome reagent for efficient transfection of mammalian cells, Biochem. Biophys. Res. Commun. 179 (1991) 280–285.
[2] J.P. Vigneron, N. Oudrhiri, M. Fauquet, L. Vergely, J.C. Bradley, M. Basseville, P. Lehn, J.M. Lehn, Guanidinium–cholesterol cationic lipids: efficient vectors for the transfection of eukaryotic cells, Proc. Natl. Acad. Sci. U. S. A. 93 (1996) 9682–9686.
[3] X. Zhou, L. Huang, DNA transfection mediated by cationic liposomes containing lipopolylysine: characterization and mechanism of action, Biochim. Biophys. Acta 1189 (1994) 195–203.
[4] H. Farhood, X. Gao, K. Son, Y.Y. Yang, J.S. Lazo, L. Huang, J. Barsoum, R. Bottega, R.M. Epand, Cationic liposomes for direct gene transfer in therapy of cancer and other diseases, Ann. N.Y. Acad. Sci. 716 (1994) 23–34.
[5] H. Farhood, N. Serbina, L. Huang, The role of dioleoyl phosphatidylethanolamine in cationic liposome mediated gene transfer, Biochim. Biophys. Acta 1235 (1995) 289–295.
[6] G.J. Nabel, E.G. Nabel, Z.Y. Yang, B.A. Fox, G.E. Plautz, X. Gao, L. Huang, S. Shu, D. Gordon, A.E. Chang, Direct gene transfer with DNA–

liposome complexes in melanoma: expression, biologic activity, and lack of toxicity in humans, Proc. Natl. Acad. Sci. U. S. A. 90 (1993) 11307–11311.
[7] E.G. Nabel, Z. Yang, D. Muller, A.E. Chang, X. Gao, L. Huang, K.J. Cho, G.J. Nabel, Safety and toxicity of catheter gene delivery to the pulmonary vasculature in a patient with metastatic melanoma, Hum. Gene Ther. 5 (1994) 1089–1094.
[8] T. Endo, K. Inoue, S. Nojima, T. Sekiya, K. Ohki, Y. Nozawa, Electron microscopic study on the structures formed by mixtures containing synthetic glyceroglycolipids, J. Biochem. (Tokyo) 93 (1983) 1–6.
[9] T.M. Allen, C. Hansen, J. Rutledge, Liposomes with prolonged circulation times: factors affecting uptake by reticuloendothelial and other tissues, Biochim. Biophys. Acta 981 (1989) 27–35.
[10] Y. Inoh, D. Kitamoto, N. Hirashima, M. Nakanishi, Biosurfactants of MEL-A increase gene transfection mediated by cationic liposomes, Biochem. Biophys. Res. Commun. 289 (2001) 57–61.
[11] D. Kitamoto, H. Yanagishita, T. Shinbo, C. Kamisawa, T. Nakane, T. Nakahara, Surface active properties and antimicrobial activities of mannosylerythritol lipids as biosurfactants produced by *Candida antarctica*, J. Biotechnol. 29 (1993) 91–96.
[12] D. Kitamoto, G. Sangita, G. Ourisson, Y. Nakatani, Formation of giant vesicles from diacylmannosylerythritols, and their binding to concanavalin A, Chem. Commun. (2000) 861–862.
[13] Isoda, H. Shinmoto, D. Kitamoto, M. Matsumura, T. Nakahara, Differentiation of human promyelocytic leukemia cell line HL60 by microbial extracellular glycolipids, Lipids 32 (1997) 263–271.
[14] Y. Wakamatsu, X. Zhao, C. Jin, N. Day, M. Shibahara, N. Nomura, T. Nakahara, T. Murata, K.K. Yokoyama, Mannosylerythritol lipid induces characteristics of neuronal differentiation in PC12 cells through an ERK-related signal cascade, Eur. J. Biochem. 268 (2001) 374–383.
[15] Y. Inoh, D. Kitamoto, N. Hirashima, M. Nakanishi, Biosurfactant MEL-A dramatically increases gene transfection via membrane fusion, J. Control. Release 94 (2004) 423–431.
[16] Y. Hattori, Y. Maitani, Enhanced in vitro DNA transfection efficiency by novel folate-linked nanoparticles in human prostate cancer and oral cancer, J. Control. Release 97 (2004) 173–183.
[17] M. Nakanishi, New strategy in gene transfection by cationic transfection lipids with a cationic cholesterol, Curr. Med. Chem. 10 (2003) 1289–1296.
[18] I.M. Banat, R.S. Makkar, S.S. Cameotra, Potential commercial applications of microbial surfactants, Appl. Microbiol. Biotechnol. 53 (2000) 495–508.
[19] S.S. Cameotra, R.S. Makkar, Synthesis of biosurfactants in extreme conditions, Appl. Microbiol. Biotechnol. 50 (1998) 520–529.

Intracellular Delivery of Proteins in Complexes with Oligoarginine-Modified Liposomes and the Effect of Oligoarginine Length

Masahiko Furuhata,† Hiroko Kawakami,‡ Kazunori Toma,‡ Yoshiyuki Hattori,† and Yoshie Maitani*,†

Institute of Medicinal Chemistry, Hoshi University, Shinagawa-ku, Tokyo 142-8501, Japan, and The Noguchi Institute, Itabashi-ku, Tokyo 173-0003, Japan. Received February 13, 2006; Revised Manuscript Received June 5, 2006

The intracellular delivery of proteins using cell-penetrating peptides (CPPs) including oligoarginine (oligo-Arg) carriers raises the possibility of establishing novel therapeutic methods. We compared the effect of the length of oligo-Arg in modified liposomes ($(Arg)_n$-L; n = 4, 6, 8, 10) on the delivery of proteins by flow cytometry, fluorescence microscopy, and spectrofluorimetry. As a free liposome, Arg4-modified liposome Arg4-L was most efficiently internalized in cells. The efficiency decreased depending on the length of oligo-Arg. For the intracellular delivery of proteins, $(Arg)_n$-L was physically associated with proteins. Concerning the effect of oligo-Arg length, liposome/protein complexes showed a different behavior. Arg4-L carried bovine serum albumin (BSA, 66 kDa) and β-galactosidase (β-Gal, 120 kDa) 6-fold higher than free BSA and free β-Gal. Arg10-L showed similar performance for these two proteins to Arg4-L. The enzymatic activity of β-Gal in the cells showed that proteins were transported as a biologically active form. Arg10-L carried 100-fold more immunoglobulin G (IgG, 150 kDa) than free IgG, and 3-fold more than Arg4-L into cells. Shorter oligo-Arg chain on liposomes may be enough for liposomes alone to be taken up in cells, but more Arg residues may be needed to form a complex with high molecular weight proteins and deliver them into cells. This information will aid in the design of $(Arg)_n$-L as a carrier for delivering proteins into cells.

INTRODUCTION

The development of therapeutic peptides and proteins is hampered by their poor ability to penetrate the plasma membrane because of their high hydrophilicity and molecular weight. Therefore, it is necessary to construct an efficient protein delivery system. One approach to solve this problem is to incorporate short peptides derived from protein-transduction domains (PTDs) or cell-penetrating peptides (CPPs), such as HIV-1 Tat fragments, penetratin and VP22. PTDs or CPPs are less than 30 amino acid residues in length and have the capability of crossing the plasma membrane (*1*−*6*). Since the PTDs and CPPs can deliver conjugated molecules, such as proteins, into cells (*7*, *8*), they are usually used as conjugates with cargo molecules, as part of a very strong and specific complex with biotin (*9*). However, these CPP carriers require cross-linking to the target peptide or protein. The only exception is pep-1, which has been reported to deliver a variety of peptides and proteins into several cell lines by forming physical assemblies without covalent chemical coupling (*6*). Since CPP-modified nanoparticles (*10*) and liposomes (*11*) can be taken up into cells, liposomes modified with Tat and penetratin were utilized in the intracellular delivery of drugs by entrapping the drugs in the liposomes (*12*). However, in the case of proteins, it is hard for them to be released from the liposomes, even if the liposomes are internalized in cells.

We synthesized oligo-Arg conjugates with an artificial lipid, and they were incorporated in liposomes for a protein delivery study. In our system, the surface of liposomes were modified with oligo-Arg ($(Arg)_n$-L; n = 4, 6, 8, 10), and proteins were physically associated on the surface. Cargo proteins were not entrapped in the liposomes. Therefore, the preparation of the complex between proteins and $(Arg)_n$-L is simple. Although investigations delineating the influence of Arg length on the uptake of oligo-Args alone have been reported (*5*, *13*−*15*), to our knowledge there is no report on $(Arg)_n$-L as a protein delivery system. $(Arg)_n$-L provides two characteristic interactions; a hydrophobic one by liposome, and a positively charged and hydrophilic one by (Arg)n. These two kinds of interactions were expected to help forming complexes with proteins.

The aim of this study is first to show that our system can transport proteins into cells, and then to examine the effect of oligo-Arg length on the protein delivery in human cervical carcinoma HeLa cells. Cellular uptake efficacy was evaluated by flow cytometry, spectrofluorimetry, and fluorescence microscopic observation of the cells. We also analyzed the interaction of $(Arg)_n$-L with proteins by fluorescence intensity distribution analysis (FIDA).

Our studies showed that the effect of oligo-Arg length on the intracellular delivery of proteins by $(Arg)_n$-L/protein complexes was different from that of $(Arg)_n$-L alone. Short oligo-Arg was enough for liposomes to be taken up into the cells, but longer oligo-Arg may be needed to form a complex with large proteins and deliver them into the cells.

EXPERIMENTAL PROCEDURES

Materials. All amino acid derivatives and coupling reagents were obtained from Kokusan Chemical Co., Ltd. (Tokyo, Japan). Egg phosphatidylcholine (EPC) was purchased from Q. P. Co., Ltd. (Tokyo, Japan). Cholesterol (Chol) and bovine serum albumin (BSA) were purchased from Wako Pure Chemical Industries, Ltd. (Osaka, Japan). Calcein was obtained from Tokyo Kasei Kogyo Co., Ltd. (Tokyo, Japan). Fluorescein isothiocyanate-labeled BSA (FITC−BSA), stearylamine, 3β-[*N*-(dimethylaminoethane)carbamoyl]cholesterol (DC−Chol), 5-(*N*-ethyl-*N*-isopropyl)amiloride (EIPA), phorbol 12-myristate 13-acetate (PMA) were from Sigma Chemical Co. (St. Louis, MO). FITC-immunoglobulin G (FITC−IgG) was provided by

* Corresponding author. Fax/phone: +81-3-5498-5048; e-mail: yoshie@hoshi.ac.jp.
† Hoshi University.
‡ The Noguchi Institute.

10.1021/bc060034h CCC: $33.50
Published on Web 07/06/2006

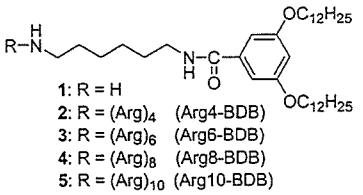

Figure 1. Chemical structures of $(Arg)_n$-BDBs.

MP Biomedicals Co. (Irvine, CA). IgG was obtained from Oriental Yeast Co., Ltd. (Tokyo, Japan). β-Galactosidase (β-Gal) and the β-Gal staining kit were purchased from Active Motif, Inc. (Carlsbad, CA). Lumi-Gal 530 (Reporter assay kit of β-Gal) was from Toyobo Co., Ltd. (Osaka, Japan). Bicinchonic acid (BCA) protein assay reagent was obtained from Pierce (Rockford, IL). Dulbecco's modified Eagle's medium (DMEM) was purchased from Invitrogen Co. (Carlsbad, CA). Fetal bovine serum (FBS) was provided by Life Technologies (Grand Island, NY). 1,1′-Dioctadecyl-3,3,3′,3′-tetramethylindocarbocyanine perchlorate (DiI) was obtained from Lambda Probes & Diagnostics (Graz, Austria). All other reagents were of analytical grade.

Synthesis of $(Arg)_n$-BDBs. $(Arg)_n$-BDBs (**2**, **3**, **4**, and **5**) were synthesized similarly to other peptide–lipid conjugates of different amino acid sequences (*16*) (Figure 1). The oligo-Arg portion was extended similarly to the compounds with a PEG linker between oligo-Arg and BDB (*17*). For example, N^{α}-9-fluorenylmethoxycarbonyl-N^{g}-2,2,5,7,8-pentamethylchroman-6-sulfonyl-L-arginine (Fmoc-Arg(Pmc)-OH) was condensed with *N*-(6-aminohexyl)-3,5-bis(dodecyloxy)benzamide (**1**) by 2-(1*H*-benzotriazol-1-yl)-1,1,3,3-tetramethyluronium hexafluorophosphate and 4-(dimethylamino)pyridine in *N*,*N*-dimethylformamide, and the Fmoc protecting group was removed by piperidine. This amide condensation and Fmoc deprotection cycle was repeated four times to give the side chain protected **2**. MALDI-TOFMS (α-CHCA): found, 2280.24; calculated for $[M + H]^+$, 2278.33. Final trifluoroacetic acid deprotection of Pmc gave **2**. MALDI-TOFMS (α-CHCA): found, 1214.99; calculated for $[M + H]^+$, 1213.94.

Cell Culture. HeLa cells were kindly provided by Toyobo Co., Ltd. (Osaka, Japan). HeLa cells were grown in DMEM supplemented with 10% FBS at 37 °C in a humidified 5% CO_2 atmosphere.

Preparation of Liposomes. Four liposomal formulas were used: EPC, Chol, and $(Arg)_n$-BDB in a molar ratio of 7:3:0.05 or 7:3:0.5 for the oligo-Arg-modified liposome ($(Arg)_n$-L); EPC and Chol in a molar ratio of 7:3 for the control liposome (Con-L); EPC, Chol, and stearylamine in a molar ratio of 7:3:2 for the stearylmaine modified liposome (SA-L); EPC, Chol, and DC–Chol in a molar ratio of 7:3:0.5 for the DC–Chol modified liposome (DC-L) for the control liposomes containing cationic lipids. Liposomes were prepared by a dry film method with water or 20 mM calcein. For $(Arg)_n$-L, $(Arg)_n$-BDB, Chol, and EPC were dissolved in an appropriate volume of chloroform, which was then removed. The particle size distributions and the zeta-potentials were measured by the dynamic and the electrophoresis light scattering method, respectively (ELS-800, Otsuka Electronics Co., Ltd., Osaka, Japan), at 25°C, after the dispersion was diluted to an appropriate volume with water. pH titration of the zeta-potential was measured by Automatic Titrator GT-06 (Mitsubishi Chemical Corporation, Tokyo, Japan). For liposomes with calcein entrapped, this was followed by chromatography on Sephadex G-50 columns, and fractions of liposomes were collected. DiI-labeled liposomes were prepared as described above but with post-addition of DiI at 0.04 mol % of total lipids.

Uptake Experiments Using Flow Cytometry. An aqueous solution of FITC–BSA, FITC–IgG, or β-Gal was added to the $(Arg)_n$-L suspension with gentle shaking to form $(Arg)_n$-L/protein complexes. Each complex was left at room temperature for 10–15 min. Cell cultures were prepared by plating cells in a 35-mm culture dish 24 h prior to each experiment. The cells were washed three times with 1 mL of serum-free DMEM. Calcein-entrapped $(Arg)_n$-L (100 μg) alone or each $(Arg)_n$-L/protein complex ($(Arg)_n$-BDB: 5 μg of protein, from 50:1 to 1000:1 molar ratio), was diluted with serum-free DMEM to 1 mL and then gently applied to the cells. In this study, all samples were incubated with cells for 3 h at 37 °C in serum-free DMEM. At the end of the incubation of $(Arg)_n$-L/protein complexes or calcein-entrapped $(Arg)_n$-L with cells, the cells were washed three times with 1 mL of PBS and detached by incubating with 0.05% trypsin and EDTA solution at 37 °C for 3 min. The cells were centrifuged at 1500*g*, and the supernatant was discarded. The cells were resuspended with PBS (pH 7.4) containing 0.1% BSA and 1 mM EDTA and directly introduced into a FACS-Calibur flow cytometer (Becton Dickinson, San Jose, CA) equipped with a 488 nm argon ion laser. Data for 10000 fluorescent events were obtained by recording forward scatter (FSC) and side scatter (SSC) with green (for FITC and calcein; 530/30 nm) and red (for DiI; 585/42 nm) fluorescence. To investigate the cellular uptake mechanism, cells were washed with serum-free medium and preincubated for 30 min at 37 °C with EIPA (25 μM) or PMA (1 μM). Subsequent incubation of the complex was carried out in the presence of the respective pharmacological reagents.

Spectrofluorimetric Quantification of Internalized FITC–BSA and IgG. At the end of the incubation of $(Arg)_n$-L/FITC-protein complexes with cells as described above, the cells were washed three times with 1 mL of PBS and lysed by incubating with 0.2% Triton X-100/PBS at 37 °C for 5 min, followed by centrifugation at 15000 rpm for 15 min. The supernatants were measured with a chemoluminometer (Ex = 485, Em = 535 nm) (Wallac ARVO SX 1420 multilabel counter, Perkin-Elmer Life Science, Japan, Co. Ltd., Kanagawa, Japan).

Fluorescence Microscopy. At the end of the incubation of $(Arg)_n$-L/protein complexes with cells as described in Uptake Experiments using Flow Cytometry, the cells were washed five times with 1 mL of PBS. Unfixed cells were observed with an Eclipse TS100/100-F for epifluorescence observations (Nicon, Tokyo, Japan). The level of contrast and the brightness of the images were adjusted.

***β*-Galactosidase Assay.** For the β-galactosidase assay, we used X-Gal staining and chemiluminescence measurements. For X-Gal staining, at the end of the incubation of $(Arg)_n$-L/β-Gal complex with cells as described in Uptake Experiments using Flow Cytometry, the cells were stained with the β-Gal staining kit and then observed with an Eclipse TS100/100-F for epifluorescence observations. The level of contrast and the brightness of the images were adjusted. For chemiluminescence measurements, β-Gal activity was measured according to the instructions accompanying the β-Gal assay system. Incubation of $(Arg)_n$-L/β-Gal complex with cells was terminated by washing the plates three times with cold PBS (pH 7.4). Cell lysis solution (Reporter assay kit of β-Gal) was added to the cell monolayers and subjected to freezing at −80 °C and thawing at 37 °C, followed by centrifugation at 15000 rpm for 2 min. Aliquots of 20 μL of the supernatants were mixed with 180 μL of Lumi-Gal 530 and then incubated for 30 min at 37 °C, and counts per second (cps) were measured with a chemoluminometer (Wallac ARVO SX 1420 multilabel counter). The protein concentration of the supernatants was determined with BCA reagent using BSA as a standard, and cps/μg protein was calculated.

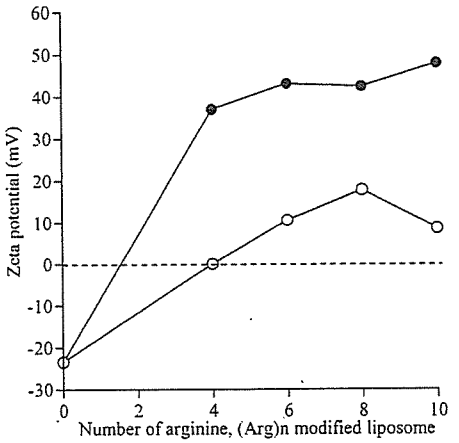

Figure 2. Effect of arginine number of $(Arg)_n$-L on the zeta potential. Open circle, liposome contained 0.5 mol % of oligo-Arg-BDB; Closed circle, liposome contained 5 mol % of oligo-Arg-BDB

Fluorescence Intensity Distribution Analysis (FIDA). FIDA was performed with a MF20 microplate reader (Olympus Corp. Tokyo, Japan) using the onboard 633-nm helium−neon laser at a power of 300 μW for excitation. Experiments were performed in 384-well glass-bottom plates using a sample volume of 50 μL. The FIDA data was analyzed with the MF20 software package. All single-molecule FIDAs were performed under identical conditions with respect to incubation (10 min) at room temperature. Protein-binding experiments were performed using the DiI-labeled Arg4-L and Arg10-L. The concentration of the labeled component was held constant whereas the concentration of BSA or IgG was varied in water.

Cytotoxicity. HeLa cells were seeded at a density of 1×10^4 cells per well in 96-well plates and maintained for 24 h before transfection in DMEM supplemented with 10% FBS. The cells were washed with PBS. The culture medium was replaced with serum-free DMEM (100 μL) including $(Arg)_n$-L/protein complex ($(Arg)_n$-BDB: 5 μg of protein = 50:1, molar ratio). After incubation for 3 h at 37 °C with serum-free DMEM (100 μL), the number of surviving cells was determined by a WST-8 assay (Dojindo Laboratories, Kumamoto, Japan). Cell viability was expressed as the ratio of the A_{450} of cells treated with the protein complex to that of the control samples.

Data Analysis. Significant differences in the mean values were evaluated using Student's unpaired *t*-test. A *p*-value of less than 0.05 was considered significant.

RESULTS

Characterization of $(Arg)_n$-L. We prepared five kinds of liposomes; a control liposome (Con-L) consisting of EPC and Chol at a molar ratio of 7:3, two positively charged control liposomes consisting of EPC, Chol, stearylamine or DC−Chol at a molar ratio of 7:3:2 or 0.5 (SA-L, DC-L, respectively), and two $(Arg)_n$-L (n = 4, 6, 8, 10) differing in $(Arg)_n$-BDB content, a molar ratio of EPC, Chol, and $(Arg)_n$-BDB at 7:3:0.05 and 7:3:0.5. Each particle size was adjusted to about 200 nm by sonication. To examine whether the liposomes were modified with Arg, we measured their zeta potential. Con-L was negatively charged, and the two $(Arg)_n$-L were positively charged (Figure 2). SA-L and DC-L were positively charged (over 50 mV in zeta potential, data not shown). The longer oligo-Arg had a higher zeta-potential, corresponding to the number of Arg residues. The zeta-potential of $(Arg)_n$-L containing 5 mol % of oligo-Arg lipid was higher than that of preparation containing 0.5 mol % (Figure 2). We used $(Arg)_n$-L containing 5 mol % of oligo-Arg lipid in the subsequent experiments, because we thought that highly positively charged carriers were desirable to form complexes with proteins and to deliver them into cells.

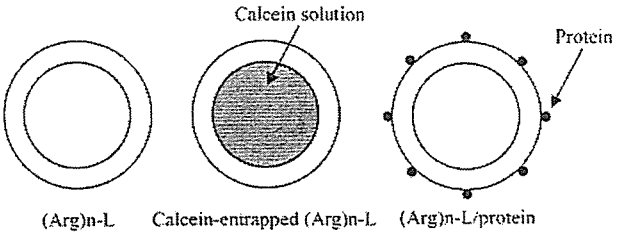

Figure 3. Schematic diagrams of the $(Arg)_n$-L, calcein-entrapped $(Arg)_n$-L and $(Arg)_n$-L/protein complex. ($(Arg)_n$-BDB in $(Arg)_n$-L): protein = 50:1, molar ratio.

Cellular Uptake of Calcein-Entrapped $(Arg)_n$-L, and $(Arg)_n$-L/FITC−BSA, and $(Arg)_n$-L/FITC−IgG Complexes. To examine the cellular uptake of $(Arg)_n$-L or the complex, cells were exposed to calcein-entrapped $(Arg)_n$-L alone, and $(Arg)_n$-L/FITC−BSA and $(Arg)_n$-L/FITC−IgG complexes for 3 h at 37 °C. Then, the cells were trypsinized and analyzed by flow cytometry. The cellular uptake of calcein-entrapped $(Arg)_n$-L decreased as the number of arginine residues increased (Figure 4A). The size of Arg4-L and Arg10-L was about 233 nm. The size of Arg4-L/FITC−BSA and FITC−IgG, and Arg10-L/FITC−BSA and FITC−IgG was about 289 nm, indicating that proteins were adhered to the surface of liposomes as schematically shown in Figure 3. The zeta potential of Arg10-L/BSA and Arg10-L/IgG was similar to that of Arg10-L at pH 3−11 when measured by the pH titration method (data not shown).

Free FITC−BSA, Con-L/FITC−BSA, SA-L/FITC−BSA, and DC-L/FITC−BSA were scarcely taken into the cell (Figure 4B). FITC−BSA in a complex with Arg4-L, Arg6-L, Arg8-L, and Arg10-L displayed a marked increase in fluorescence in the cells, showing about a 6-, 5-, 3-, and 6-fold higher intensity, respectively, than free FITC−BSA. Arg4-L and Arg10-L were most efficient at delivering FITC−BSA into the cells.

Free FITC−IgG (150 kDa), Con-L/FITC−IgG, SA-L/FITC−IgG, and DC-L/FITC−IgG complexes were scarcely taken up at all (Figure 4C). FITC−IgG in a complex with Arg4-L, Arg6-L, Arg8-L, and Arg10-L showed about 30-, 100-, 60-, and 100-fold greater cellular uptake, respectively, than free FITC−IgG. Arg6-L and Arg10-L showed the greatest efficiency in delivering FITC−IgG. However, FITC−IgG and Arg10-L without complex formation showed less cellular uptake of FITC−IgG than Arg4-L/FITC−IgG (data not shown).

We assayed the cellular internalization of the Arg4-L and Arg10-L/FITC−BSA or FITC−IgG complexes for a quantitative evaluation of the amount of internalized protein. Cells were exposed to the same conditions as for the flow cytometric analysis and lysed by 0.2% Triton X-100/PBS. FITC−BSA (5 μg/mL) was internalized in the cells at about 40% and 30% of the dose with Arg4-L and with Arg10-L, respectively. On the other hand, FITC−IgG was internalized at about 10% and 19% of the dose with Arg4-L and with Arg10-L, respectively.

Efficiency of the Cellular Uptake of Arg10-L/FITC−IgG Based on the Ratio of Arg10-L to IgG. We examined the optimal molar ratio of Arg10-BDB to IgG in the Arg10-L/FITC−IgG complex, assaying the cellular internalization of various Arg10-L/FITC−IgG complexes by flow cytometry (Figure 5). Here, the molar ratio of Arg10-L/FITC−IgG refers to the ratio of Arg10-BDB to FITC−IgG because the proportion of Arg10-BDB in liposomes was constant (5 mol %). Cells were exposed for 3 h to the Arg10-L/FITC−IgG complex and then trypsinized. The cellular uptake of FITC−IgG increased as the molar ratio of Arg10-L/FITC−IgG increased and seemed to reach a level of saturation above a molar ratio of 100. It could

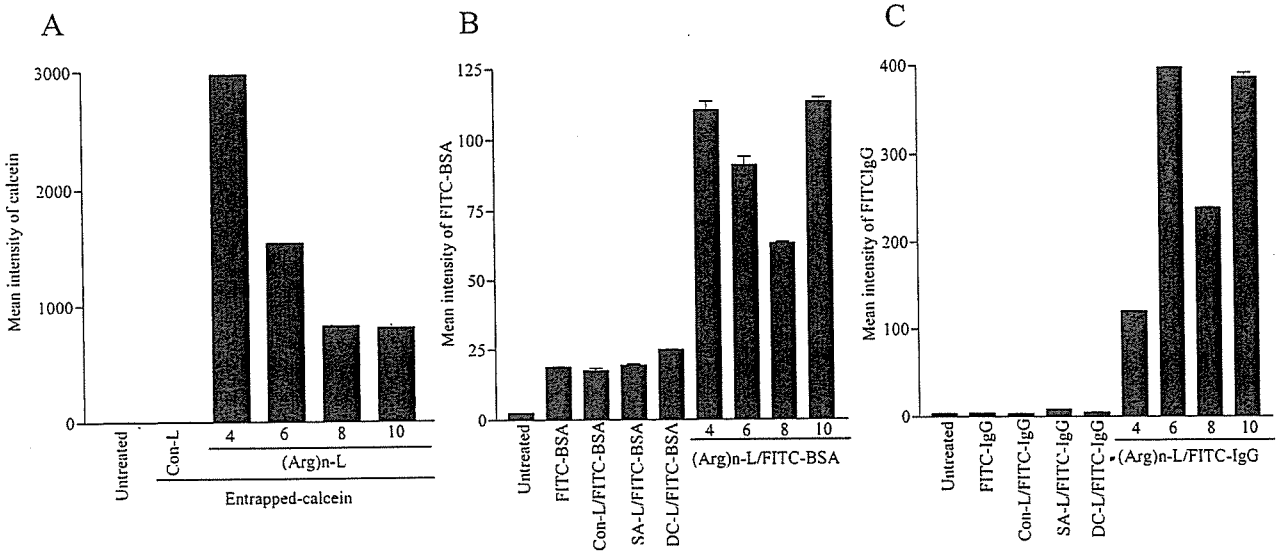

Figure 4. Cellular uptake of the calcein-entrapped $(Arg)_n$-L (A), and $(Arg)_n$-L in complexes with FITC−BSA (B) and FITC−IgG (C). Calcein-entrapped $(Arg)_n$-L (100 μg) alone or each $(Arg)_n$-L/protein complex (a variable $(Arg)_n$-BDB: 5 μg of FITC−BSA or FITC−IgG = 50:1, molar ratio) was diluted with serum-free DMEM to 1 mL and then gently applied to the cells, incubated with the cells for 3 h at 37 °C in serum-free DMEM, and treated with trypsin before FACS analysis. Con-L exhibits liposome without $(Arg)_n$-BDB. SA-L and DC-L exhibit liposome with stearylamine and DC−Chol, respectively. Each value is the mean ± SD of three separate determinations.

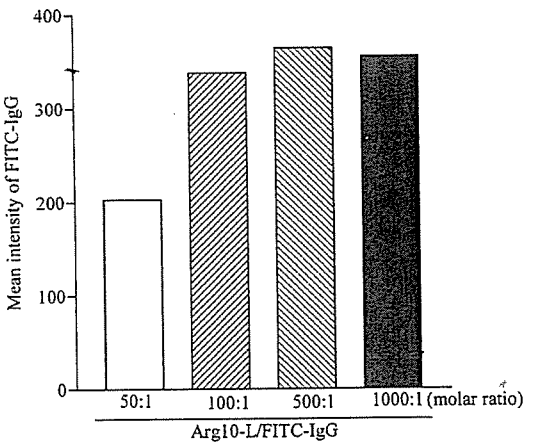

Figure 5. Cellular uptake of the Arg10-L/FITC−IgG complex as a function of the molar ratio between Arg10-BDB and FITC−IgG. Arg10-L/FITC−IgG (a variable Arg10-BDB: 5 μg of FITC−IgG, molar ratio from 50:1 to 1000:1) was diluted with serum-free DMEM to 1 mL and then gently applied to the cells and incubated with the cells at 37 °C for 3 h in serum-free DMEM and treated with trypsin before FACS analysis. Each value is the mean ± SD of three separate determinations.

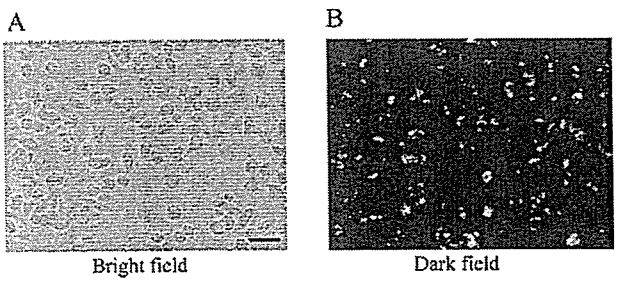

Figure 6. Analysis of FITC−IgG uptake by fluorescence microscopy. Arg10-L/FITC−IgG complex (Arg10:5 μg of FITC−IgG = 100:1, molar ratio) was diluted with serum-free DMEM to 1 mL, gently applied to the cells, and then incubated with the cells for 1 h at 37 °C in serum-free DMEM. The unfixed cells were observed with a fluorescence microscope (magnification × 200). Scale bar = 50 μm.

deliver about 1.5-fold more at a molar ratio of 100 than at 50 without change in the size of the complex.

To confirm the internalization and localization of FITC−IgG in the unfixed cells, we observed the cells by fluorescence microscopy after exposing them to the Arg10-L/FITC−IgG (100: 1) complex for 3 h and washing them five times (Figure 6A, B). FITC−IgG was observed to be taken into almost all cells.

Cellular Uptake of $(Arg)_n$-L/β-Gal Complexes. To examine whether the internalized protein is functional, we observed the enzymatic activity of β-Gal by microscopy. Cells were exposed to the Arg4-L and Arg10-L/β-Gal complexes for 3 h at 37 °C. Then, we observed the efficiency of protein delivery by monitoring the enzymatic activity of β-Gal using X-Gal staining (Figure 7). The cells treated with free β-Gal gave a similar image to untreated cells, suggesting that free β-Gal did not enter the cells (Figure 7A,B). About 70% and 50% of cells with Arg4-L and with Arg10-L, respectively, exhibited strong and uniform β-Gal activity (Figure 7C,D). At a higher magnification, we could confirm that β-Gal activity was present in the cytoplasm (Figure 7E,F). The β-Gal activity in the cells treated with Arg4-L and Arg10-L was about 5.9-fold and 4.4-fold stronger, respectively, than that of cells treated with free β-Gal, and β-Gal (5 μg/mL) was internalized in the cells at about 9.7% and 7.2% of the dose with Arg4-L and with Arg10-L, respectively in the chemiluminescence assay. Most notably, the presence of Arg4-L or Arg10-L did not alter the enzymatic activity of β-Gal upon delivery into cells. Arg4-L could deliver β-Gal (120 kDa) more efficiently than Arg10-L, similar to the transport of FITC−BSA. No cytotoxicity was observed for all $(Arg)_n$-L or $(Arg)_n$-L/protein complexes (data not shown).

FIDA Measurements. To examine whether there is a difference in the complex formation, we used FIDA to characterize the interaction of the $(Arg)_n$-L/protein complex. FIDA allows the characterization of fluorescently labeled molecules with respect to their molecular brightness and concentration at the single-molecule level (*18*). Briefly, the FIDA method is based on the collected photon numbers recorded in time intervals of fixed duration (time windows). Using this information, a count number histogram is built up. Then, a theoretical probability distribution of photon numbers is fitted against the obtained histogram, yielding specific brightness values (Q), corresponding to the concentrations (C), for all

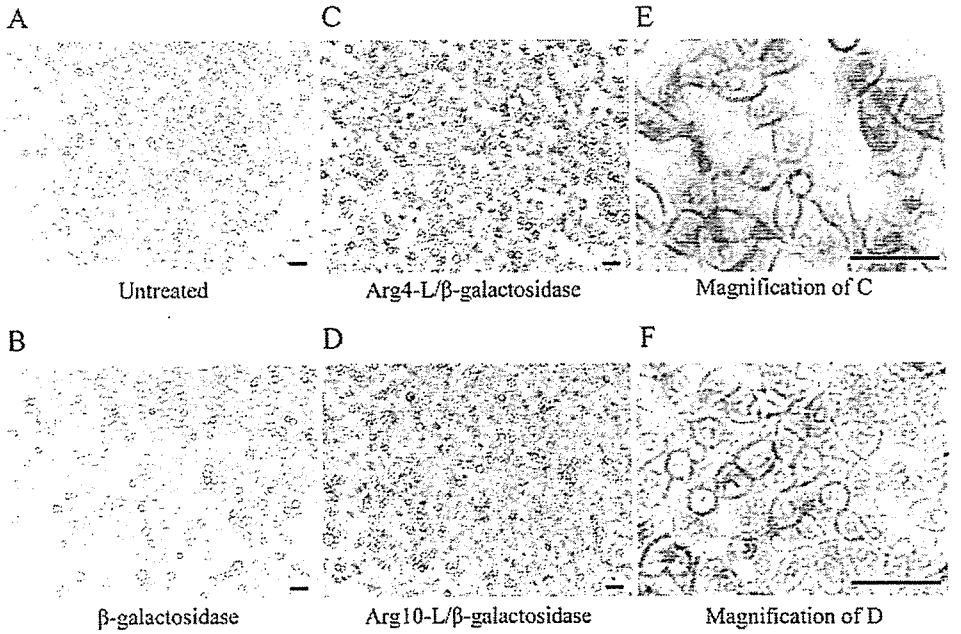

Figure 7. Analysis of β-galactosidase uptake by microscopy. Arg4-L, Arg10-L/β-galactosidase complex (Arg4-BDB or Arg10-BDB: 5 μg of β-galactosidase = 50:1, molar ratio), or 5 μg of β-galactosidase was diluted with serum-free DMEM to 1 mL and then gently applied to the cells and incubated with the cells for 1 h at 37 °C in serum-free DMEM. The cells were stained with a β-galactosidase staining kit and observed with a fluorescence microscope. Scale bar = 50 μm.

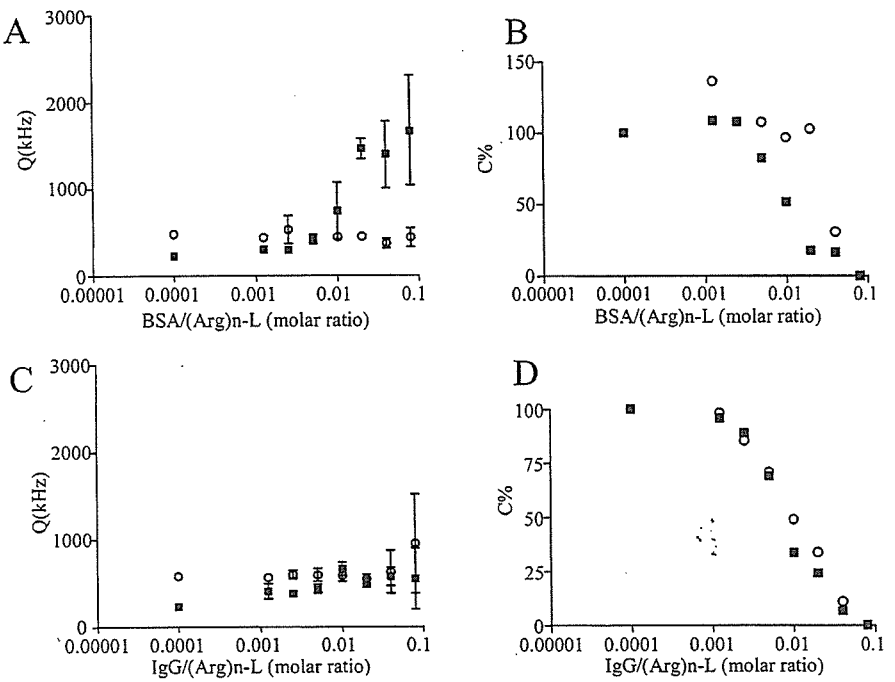

Figure 8. Fluorescence intensity distribution analysis (FIDA) of DiI-labeled Arg4- and Arg10-L/BSA or DiI-labeled Arg4-L and Arg10-L/IgG as a function of the molar ratio between Arg4- or Arg10-BDB and protein. Part A or C was the analytical result of the *Q* value. Part B or D was the analytical result of the ratio of the *C* value. Complex was diluted with water. Square, Arg4-L; Circle, Arg10-L. Each value is the mean ± SD of three separate determinations.

different species. To determine the interaction of the $(Arg)_n$-L with proteins, we measured fluorescence intensity distribution of lipid marker, DiI incorporated in the particle lipid layers as a function of the molar ratio between Arg4- or Arg10-L and protein. Here, the molar ratio of the Arg4-L or Arg10-L/protein complex refers to the ratio of Arg4- or Arg10-BDB to protein. *Q* value of Arg4-L increased at about 0.01 BSA/Arg4-L molar ratio, but that of Arg10-L did not (Figure 8A), corresponding to *C* value of Arg4-L decreased (Figure 8B). Increase of BSA might form complex with high molar ratio of Arg4-L, which increased brightness per complex (*Q* value) and decreased fluorescent Arg4-L number (*C* value). For Arg10-L, the ratio of Arg10-L/BSA in the complex was not changed in this range. Therefore, *Q* value of the complex was not changed. The interaction of IgG with Arg4-L and Arg10-L was similar (Figure 8C, D).

Mechanism of Cellular Uptake of Arg4-L, Arg10-L, and Complexes. To investigate the internalization mechanism of

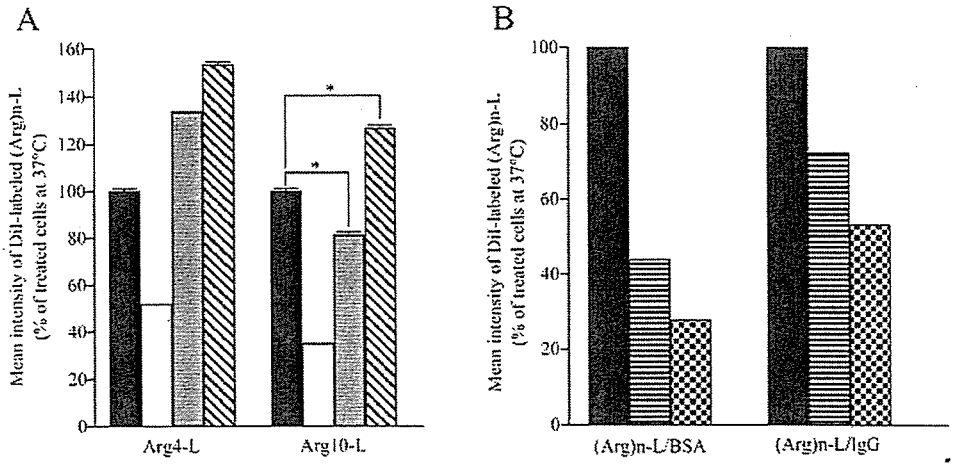

Figure 9. Effect of temperature and pharmacological reagents on the cellular uptake of DiI-labeled $(Arg)_n$-L (A) and $(Arg)_n$-L/protein complex (B). (A) HeLa cells were pretreated with EIPA (25 μM) or PMA (1 μM) at 37 °C for 30 min. The medium was replaced with fresh medium containing DiI-labeled Arg4-L or Arg10-L (100 μg/mL). The cells were incubated for 1 h at 37 °C in serum-free DMEM containing EIPA (25 μM) or PMA (1 μM) and then treated with trypsin before the flow cytometry. Dark bar, 37 °C or no pharmacological reagent; open bar, 4 °C; gray bar, EIPA; slashed bar, PMA. Each value is the mean ± SD of three separate determinations. (B) Effect of temperature on the cellular uptake of DiI-labeled Arg4-L and Arg10-L/protein complex. The experimental conditions were the same as in Figure 4B and C. Dark bar, 37 °C; sideline bar, Arg4-L at 4 °C; mosaic bar, Arg10-L at 4 °C. Each value is the mean ± SD of three independent experiments.

Arg4-L, Arg10-L and their complexes, we prepared DiI-labeled liposomes and examined the effect of temperature, a macropinocytosis inhibitor (EIPA) or an accelerator (PMA) on the cellular uptake of the liposomes. Cells were exposed to DiI-labeled Arg4-L or Arg10-L for 3 h at either 4 °C or 37 °C. Then, they were trypsinized and analyzed by flow cytometry. DiI-labeled Arg4-L and Arg10-L showed about a 50% and 65% lower internalization efficiency, respectively, at 4 °C than at 37 °C (Figure 9A). This finding suggests that the transport occurred through energy-dependent endocytosis. The cells were exposed to DiI-labeled Arg4-L or Arg10-L at 37 °C for 1 h in the absence or presence of EIPA or PMA (Figure 9A). The cellular uptake of Arg4-L increased about 34% in the presence of EIPA, and about 54% in the presence of PMA compared with untreated cells. The cellular uptake of Arg10-L significantly decreased about 20% in the presence of EIPA ($p < 0.05$), but significantly increased about 27% in the presence of PMA ($p < 0.05$) compared with untreated cells. The inhibition of cellular uptake at 4 °C for the Arg4-L/protein complex was lower than that for the Arg10-L/protein complex (Figure 9 B). This finding suggests that Arg4-L and Arg10-L/protein were taken up via an endocytotic pathway as well as Arg4-L or Arg10-L alone.

DISCUSSION

As a free liposome, Arg4-L was most efficiently internalized in the cells. The efficiency decreased depending on the length of oligo-Arg. To our knowledge, this may be the first experimental demonstration that the liposomes with shorter oligo-Arg-L alone were internalized more efficiently than those with longer ones. Besides the demonstration of the free $(Arg)_n$-L cellular uptake, our study reveals protein delivery by $(Arg)_n$-L. Concerning the effect of oligo-Arg length, liposome/protein complexes showed a different trend.

Generally, the cellular uptake of oligo-Arg increases in efficiency as the number of arginine residues increases (*5*). Both Tat and penetratin enhanced the efficiency of the uptake of liposomes in proportion to the number of peptides attached to the liposomal surface (*12*). In our experiments, the shorter oligo-Arg system, Arg4-L, penetrated the cells more efficiently than the longer one, Arg10-L, in the case of calcein-entrapped $(Arg)_n$-L.

To examine the internalization of liposomes, calcein, a water-soluble marker, was entrapped in $(Arg)_n$-L. Liposome−cell interaction on the surface might lead to the leakage of calcein due to liposome destabilization. However, the calcein leakage from $(Arg)_n$-L was small (data not shown). Uptake of DiI-labeled liposomes, which has label-lipid in the liposomes, also exhibited similar behavior to that of calcein-entapped liposomes (data not shown). These findings suggest that the calcein-entrapped $(Arg)_n$-L penetrated as liposomes, and that the difference in the cellular uptake of calcein corresponded to that of the liposomes.

FITC−BSA (66 kDa), β-Gal (120 kDa), and FITC−IgG (150 kDa) were used as model proteins. Cellular uptake of FITC−BSA was increased three to six times when it was in a complex with $(Arg)_n$-L. The highest level of cellular uptake of FITC−BSA was observed with Arg4-L and Arg10-L. For β-Gal, Arg4-L carried β-Gal 6-fold higher than free one. Arg4-L could deliver β-Gal more efficiently than Arg10-L. The enzymatic activity of β-Gal showed a protein to be transported as a biologically active protein. For FITC−IgG, Arg10-L gave the best result.

FIDA showed that the interaction of Arg4-L with BSA was stronger than that of Arg10-L with BSA, and the interaction of Arg4-L and Arg10-L with IgG was similar. At molar ratio of BSA/DiI labeled Arg4-L > 0.02, BSA associated on the surface of liposomes may interact with DiI or the complex may be aggregated. BSA may interact hydrophobic part of Arg4-L. The efficient cellular uptake of Arg4-L/BSA may reflect the strong interaction between Arg4-L and BSA. Also, DiI-labeled Arg4-L in a complex with proteins was taken up more efficiently than Arg10-L complex (data not shown). In the case of IgG, Arg10-L delivered about 3-fold more proteins than Arg4-L (Figure 4C). Because proteins formed complexes with $(Arg)_n$-L prior to the intracellular delivery, it can be postulated that the mode of interactions between proteins and $(Arg)_n$-L might be different depending on the protein.

The cellular uptake was also examined with the fluorescence microscope. To avoid artifacts caused by the fixation procedure, we observed live cells. Fixation was shown to cause significant artifacts regarding the cellular localization (*19*). From the microscopic observation, the fluorescence of FITC−IgG was observed in almost 100% of cells when transported as the Arg10-L complex (Figure 6). From the quantitative evaluation, Arg10-L delivered about 1.2-fold of IgG compared with Arg4-L, whereas FACS analysis indicated that Arg10-L delivered

almost 3-fold more than Arg4-L. The discrepancy could be explained by the sensitivity of fluorescein emission in the microenvironment and partial quenching in the endosomal structures of live cells used for the FACS analysis (*20*).

The cellular translocation by CPP was initially proposed to be an energy-independent process, because no difference was observed in cellular uptake between 37 °C and 4 °C (*2, 5*). However, more recent papers suggest that the majority of the translocation occurs via an energy-dependent pathway, and that the translocation of CPP is reduced by endocytosis inhibitors (*21*−*23*). From the temperature-dependence, the internalization of Arg4-L and Arg10-L was shown to mainly involve endocytosis. Endocytosis represents a variety of mechanisms that fall into two broad categories, phagocytosis and pinocytosis. Phagocytosis is typically restricted to specialized mammalian cells, whereas pinocytosis occurs in most cells via at least four basic mechanisms: macropinocytosis, clathrin-mediated endocytosis, caveolae-mediated endocytosis, and clathrin- and caveolae-independent endocytosis (*24*). In the latest papers, the translocation of Tat peptide is suggested to occur through macropinocytosis which is dependent on lipidic microdomains (*25*), and that of octa-arginine (R8) peptide is also shown to involve macropinocytosis (*26*). EIPA inhibits the Na^+/H^+ exchange and has been shown to inhibit macropinocytosis (*25*). PMA is a protein kinase C activator and stimulates macropinocytosis by increasing membrane ruffles (*27*−*30*). The change in cellular uptake of Arg4-L and Arg10-L caused by a macropinocytosis inhibitor (EIPA) or an accelerator (PMA) suggests that the internalization of Arg10-L occurs mainly through macropinocytosis. Since the cellular translocation of Arg4-L did not decrease by EIPA, it might involve a different mechanism than macropinocytosis.

Pep-1 can efficiently deliver proteins into cells by forming physical assemblies with a variety of proteins at the optimal molar ratio of pep-1 and a protein (*6, 31*). The internalization of pep-1 alone and pep-1/β-Gal complex is not dependent on the endocytotic pathway (*6*). The cellular uptake of the Arg10-L/FITC−IgG complex was greatly enhanced starting from a molar ratio of 50 up to 100 and reached a plateau thereafter. The difference in the behavior of pep-1 and Arg10-L concerning the molar ratio with a protein might also suggest differences in their uptake mechanism.

The most striking result of the present study is that the simple complex formation between oligo-Arg-modified liposomes and proteins, without the entrapment of proteins in the internalized space of liposomes, can produce a cellular transportable protein delivery system, which can deliver active proteins into cells. $(Arg)_n$-L will be useful to deliver macromolecules, which are difficult to entrap in liposomes, into cells. Furthermore, it could release proteins in the cytoplasm because proteins bind on the outer surface of the liposomes. A short oligo-Arg on $(Arg)_n$-L alone may be enough to be taken up in cells, but a longer Arg repeat might be needed to form a complex with large proteins and deliver them into cells. The most suitable (Arg)n-L for a protein delivery could be selected experimentally based on the results of $(Arg)_n$-L complexed with the protein. Such information will be helpful in the design of $(Arg)_n$-L as a carrier for delivering proteins into cells.

In summary, we synthesized $(Arg)_n$-BDB and prepared oligo-Arg modified liposomes as a novel carrier of proteins into cells. We found that the penetrating abilities of $(Arg)_n$-L alone and in complexes with proteins differed. The mechanism of cell membrane penetration of Arg4-L and Arg10-L, and their complexes with proteins, although not thoroughly understood, is probably different.

ACKNOWLEDGMENT

This project was supported in part by a grant from the Promotion and Mutual Aid Corporation for Private Schools of Japan and by a Grant-in-Aid for Scientific Research from the Ministry of Education, Culture, Sports, Science, and Technology of Japan.

LITERATURE CITED

(1) Derossi, D., Joliot, A. H., Chassaing, G., and Prochiantz, A. (1994) The third helix of the Antennapedia homeodomain translocates through biological membranes. *J. Biol. Chem. 269*, 10444−10450.

(2) Vives, E., Brodin, P., and Lebleu, B. (1997) A truncated HIV-1 Tat protein basic domain rapidly translocates through the plasma membrane and accumulates in the cell nucleus. *J. Biol. Chem. 272*, 16010−16017.

(3) Pooga, M., Hallbrink, M., Zorko, M., and Langel, U. (1998) Cell penetration by transportan. *FASEB J. 12*, 67−77.

(4) Oehlke, J., Scheller, A., Wiesner, B., Krause, E., Beyermann, M., Klauschenz, E., Melzig, M., and Bienert, M. (1998) Cellular uptake of an alpha-helical amphipathic model peptide with the potential to deliver polar compounds into the cell interior non-endocytically. *Biochim. Biophys. Acta 1414*, 127−139.

(5) Futaki, S., Suzuki, T., Ohashi, W., Yagami, T., Tanaka, S., Ueda, K., and Sugiura, Y. (2001) Arginine-rich peptides. An abundant source of membrane-permeable peptides having potential as carriers for intracellular protein delivery. *J. Biol. Chem. 276*, 5836−5840.

(6) Morris, M. C., Depollier, J., Mery, J., Heitz, F., and Divita, G. (2001) A peptide carrier for the delivery of biologically active proteins into mammalian cells. *Nat. Biotechnol. 19*, 1173−1176.

(7) Schwarze, S. R., Ho, A., Vocero-Akbani, A., and Dowdy, S. F. (1999) In vivo protein transduction: delivery of a biologically active protein into the mouse. *Science 285*, 1569−1572.

(8) Elliott, G., and O'Hare, P. (1997) Intercellular trafficking and protein delivery by a herpesvirus structural protein. *Cell 88*, 223−233.

(9) Saalik, P., Elmquist, A., Hansen, M., Padari, K., Saar, K., Viht, K., Langel, U., and Pooga, M. (2004) Protein cargo delivery properties of cell-penetrating peptides. A comparative study. *Bioconjugate Chem. 15*, 1246−1253.

(10) Lewin, M., Carlesso, N., Tung, C. H., Tang, X. W., Cory, D., Scadden, D. T., and Weissleder, R. (2000) Tat peptide-derivatized magnetic nanoparticles allow in vivo tracking and recovery of progenitor cells. *Nat. Biotechnol. 18*, 410−414.

(11) Torchilin, V. P., Rammohan, R., Weissig, V., and Levchenko, T. S. (2001) TAT peptide on the surface of liposomes affords their efficient intracellular delivery even at low temperature and in the presence of metabolic inhibitors. *Proc. Natl. Acad. Sci. U.S.A. 98*, 8786−8791.

(12) Tseng, Y. L., Liu, J. J., and Hong, R. L. (2002) Translocation of liposomes into cancer cells by cell-penetrating peptides penetratin and tat: a kinetic and efficacy study. *Mol. Pharmacol. 62*, 864−872.

(13) Mitchell, D. J., Kim, D. T., Steinman, L., Fathman, C. G., and Rothbard, J. B. (2000) Polyarginine enters cells more efficiently than other polycationic homopolymers. *J. Pept. Res. 56*, 318−325.

(14) Wender, P. A., Mitchell, D. J., Pattabiraman, K., Pelkey, E. T., Steinman, L., and Rothbard, J. B. (2000) The design, synthesis, and evaluation of molecules that enable or enhance cellular uptake: peptoid molecular transporters. *Proc. Natl. Acad. Sci. U.S.A. 97*, 13003−13008.

(15) Futaki, S., Ohashi, W., Suzuki, T., Niwa, M., Tanaka, S., Ueda, K., Harashima, H., and Sugiura, Y. (2001) Stearylated arginine-rich peptides: a new class of transfection systems. *Bioconjugate Chem. 12*, 1005−1011.

(16) Hara, M., Takanashi, Y., Tuzuki, N., Kawakami, H., Toma, K., and Higuchi, A. (2003) Production of interferon-β by NB1−RGB cells cultured on peptide-lipid membranes. *Cytotechnology 42*, 13−20.

(17) Furuhata, M., Kawakami, H., Toma, K., Hattori, Y., and Maitani, Y. (2006) Design, synthesis and gene delivery efficiency of novel oligo-arginine-linked PEG-lipids: Effect of oligo-arginine length. *Int. J. Pharm. 316*, 109−116.

(18) Kask, P., Palo, K., Ullmann, D., and Gall, K. (1999) Fluorescence-intensity distribution analysis and its application in biomolecular detection technology. *Proc. Natl. Acad. Sci. U.S.A. 96*, 13756−13761.

(19) Richard, J. P., Melikov, K., Vives, E., Ramos, C., Verbeure, B., Gait, M. J., Chernomordik, L. V., and Lebleu, B. (2003) Cell-penetrating peptides. A reevaluation of the mechanism of cellular uptake. *J. Biol. Chem. 278*, 585−590.

(20) Fischer, R., Kohler, K., Fotin-Mleczek, M., and Brock, R. (2004) A stepwise dissection of the intracellular fate of cationic cell-penetrating peptides. *J. Biol. Chem. 279*, 12625−12635.

(21) Vives, E. (2003) Cellular uptake of the Tat peptide: an endocytosis mechanism following ionic interactions. *J. Mol. Recognit. 16*, 265−271.

(22) Drin, G., Cottin, S., Blanc, E., Rees, A. R., and Temsamani, J. (2003) Studies on the internalization mechanism of cationic cell-penetrating peptides. *J. Biol. Chem. 278*, 31192−31201.

(23) Fischer, R., Waizenegger, T., Kohler, K., and Brock, R. (2002) A quantitative validation of fluorophore-labelled cell-permeable peptide conjugates: fluorophore and cargo dependence of import. *Biochim. Biophys. Acta 1564*, 365−374.

(24) Conner, S. D., and Schmid, S. L. (2003) Regulated portals of entry into the cell. *Nature 422*, 37−44.

(25) Wadia, J. S., Stan, R. V., and Dowdy, S. F. (2004) Transducible TAT-HA fusogenic peptide enhances escape of TAT-fusion proteins after lipid raft macropinocytosis. *Nat. Med. 10*, 310−315.

(26) Nakase, I., Niwa, M., Takeuchi, T., Sonomura, K., Kawabata, N., Koike, Y., Takehashi, M., Tanaka, S., Ueda, K., Simpson, J. C., Jones, A. T., Sugiura, Y., and Futaki, S. (2004) Cellular uptake of arginine-rich peptides: roles for macropinocytosis and actin rearrangement. *Mol. Ther. 10*, 1011−1022.

(27) Holm, P. K., Eker, P., Sandvig, K., and van Deurs, B. (1995) Phorbol myristate acetate selectively stimulates apical endocytosis via protein kinase C in polarized MDCK cells. *Exp. Cell Res. 217*, 157−168.

(28) Amyere, M., Payrastre, B., Krause, U., Van Der Smissen, P., Veithen, A., and Courtoy, P. J. (2000) Constitutive macropinocytosis in oncogene-transformed fibroblasts depends on sequential permanent activation of phosphoinositide 3-kinase and phospholipase C. *Mol. Biol. Cell. 11*, 3453−3467.

(29) Riezman, H., Woodman, P. G., van Meer, G., and Marsh, M. (1997) Molecular mechanisms of endocytosis. *Cell 91*, 731−738.

(30) Grimmer, S., van Deurs, B., and Sandvig, K. (2002) Membrane ruffling and macropinocytosis in A431 cells require cholesterol. *J. Cell Sci. 115*, 2953−2962.

(31) Henriques, S. T., Costa, J., and Castanho, M. A. (2005) Translocation of beta-Galactosidase Mediated by the Cell-Penetrating Peptide Pep-1 into Lipid Vesicles and Human HeLa Cells Is Driven by Membrane Electrostatic Potential. *Biochemistry 44*, 10189−10198.

BC060034H

Two-step transcriptional amplification–lipid-based nanoparticles using PSMA or midkine promoter for suicide gene therapy in prostate cancer

Yoshiyuki Hattori and Yoshie Maitani[1]

Institute of Medicinal Chemistry, Hoshi University, Ebara 2-4-41, Shinagawa-ku, Tokyo 142-8501, Japan

(Received March 13, 2006/Revised April 14, 2006/Accepted April 24, 2006/Online publication June 16, 2006)

A two-step transcriptional amplification system (TSTA) was used to enhance the efficacy of suicide gene therapy for treatment of prostate cancer. We designed a TSTA system and constructed two types of plasmid: one containing GAL4–VP16 fusion protein under the control of a tumor-specific promoter, the other containing luciferase or herpes simplex virus thymidine kinase (HSV-tk) under the control of a synthetic promoter. The TSTA systems using nanoparticles based on lipids were evaluated by measuring the amount of induced luciferase activity as a function of prostate-specific membrane antigen (PSMA) and midkine (Mk) promoters, specific for LNCaP and PC-3 prostate cancer cells, respectively. In LNCaP cells that were PSMA-positive, the TSTA system featuring the PSMA enhancer and promoter exhibited activity that was 640-fold greater than a system consisting of one-step transcription with the PSMA promoter. In contrast, this difference in activity did not occur in PSMA-negative PC-3 cells. In Mk-positive PC-3 cells, the TSTA system with the Mk promoter exhibited a five-fold increase in activity over one-step transcription, but such activity was not induced in Mk-negative LNCaP cells. When using HSV-tk for suicide gene therapy, TSTA systems featuring the PSMA or Mk promoter inhibited *in vitro* cell growth in the presence of ganciclovir. Furthermore, the TSTA system featuring the Mk promoter suppressed *in vivo* growth of PC-3 tumor xenografts to a greater extent than one-step transcription. These findings show that TSTA systems can enhance PSMA and Mk promoter activities and selectively inhibit PC-3 cell growth in tumors. This suggests that TSTA systems featuring tumor-specific promoters are suitable for cancer treatment by gene therapy. (*Cancer Sci* 2006)

Currently, many kinds of gene therapy research are being carried out, especially in the field of cancer treatment.[1] The most difficult aspect of developing an *in vivo* approach is correctly targeting cancer cells. The random delivery of a therapeutic gene damages normal cells in essential organs such as the liver, lung, kidney and spleen, and can cause death. Many vectors target tumors for gene delivery, including viral and synthetic vectors (liposome and emulsion),[2] whereas others that use tumor-specific promoters to regulate expression transcriptionally in target cancer cells have also shown promise. It is essential to use a strong and tissue-specific promoter region if a suicide gene is to be expressed selectively in the cancer cells.

Prostate cancer is the most frequently diagnosed cancer and the second leading cause of death in men in the USA, after lung cancer.[3] The prostate-specific antigen (PSA) test is carried out routinely in men to detect the presence of prostate cancer by immunoassaying the level of PSA in serum. Currently, androgen deprivation is the most effective treatment for advanced prostate cancer, but it reduces PSA serum levels,[4] affecting the utility of PSA as a prostate tumor-specific promoter. Like PSA, prostate-specific membrane antigen (PSMA) has elevated expression in prostate cancer[5] and has been reported to accumulate under conditions of androgen deprivation,[6] potentially making it a more useful tool when tracking a patient's response during prostate cancer treatment. This suggested that the PSMA promoter appears to be highly suitable for gene therapy.[7] Midkine (Mk) is a heparin-binding growth factor whose expression is regulated developmentally.[8,9] Its biological function during tumorigenesis remains unclear but Mk is expressed in various types of human cancer, including prostate cancer.[10–12] In contrast, its expression in adult tissues is strictly limited.[10] Several groups have reported that Mk promoter-mediated suicide gene therapy effectively produces cytotoxic effects in cancer cells.[13]

Both the PSMA and Mk genes have been identified as factors expressed specifically in cancer cells; however, the promoter region has one disadvantage in that it does not have strong promoter activity, which, in turn, limits the cells' ability to express the suicide gene. Suicide gene therapy with a PSA enhancer and promoter in the LNCaP model also had no significant effect with a one-step transcription system.[14] It is essential to find a way to enhance the transcriptional activity of such promoters. Several methods can potentially be used to increase levels of reporter or therapeutic proteins in prostate cancer.[15–18] One of the amplification approaches, referred to as a two-step transcriptional amplification system (TSTA), can potentially be used to improve the transcriptional activity of cellular promoters with the GAL4–VP16 fusion protein, which comprises the DNA-binding domain of the yeast transcriptional activator GAL4 and the activation domain of the herpes simplex virus 1 activator VP16 (Fig. 1). GAL4 is a transcriptional factor that regulates gene transcription tightly by binding its responsive elements. A potent transcriptional activator, GAL4–VP16, which is driven by the cell-specific promoter of an effector plasmid, acts on the promoter of a second expression plasmid (reporter plasmid), which encodes the reporter or therapeutic protein (Fig. 1). For temporally regulated expression, a tetracycline-repressible transactivator system for inducible gene expression was developed using tet-repressor fused to VP16.[19] TSTA

[1]To whom correspondence should be addressed. E-mail: yoshie@hoshi.ac.jp

doi: 10.1111/j.1349-7006.2006.00243.x

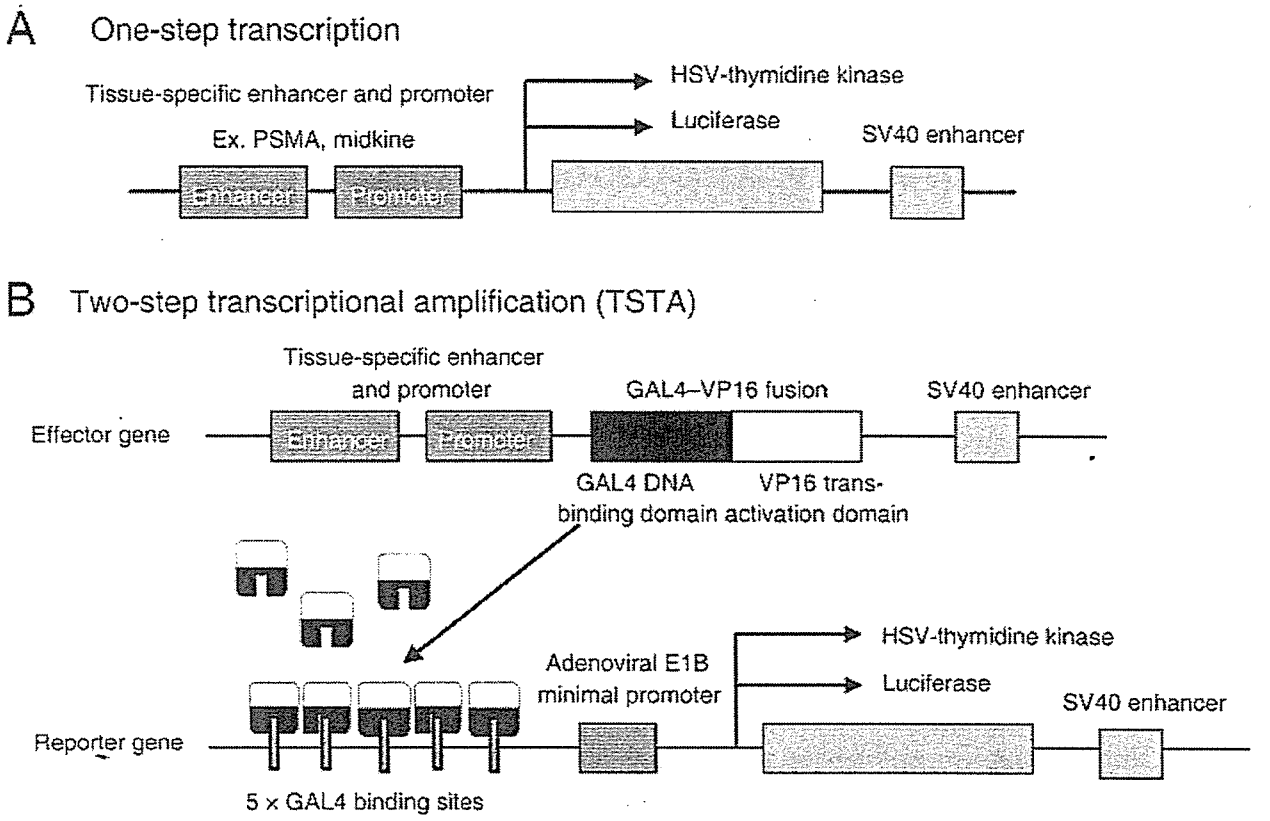

Fig. 1. Schematic diagram of (A) one-step transcription and (B) two-step transcriptional amplification (TSTA system) used in this study.[16] In the TSTA system, the first step involves the tissue-specific (e.g. prostate-specific membrane antigen [PSMA], midkine) expression of the GAL4–VP16 fusion protein. In the second step, GAL4–VP16 drives the target gene expression under the control of GAL4-binding sites and the adenoviral E1B minimal promoter. Transcription of the reporter gene, either herpes simplex virus (HSV) thymidine kinase or luciferase, leads to reporter protein. The use of the GAL4–VP16 fusion protein can potentially lead to amplified levels of the reporter protein.

systems for the amplification of tumor-specific gene expression has been reported in PSA promoter for prostate cancer,[15,16] Muc-1 promoter for colon carcinoma[20] and caricinoembryonic antigen (CEA) promoter for lung cancer and colon adenocarcinoma, respectively.[21] However, TSTA systems with PSMA and Mk promoters have not been reported, and the TSTA system has not been applied to suicide gene therapy with herpes simplex virus thymidine kinase (HSV-tk).

In the present study, we modified the TSTA system using a reporter plasmid with a combination of the adenoviral E1B minimal promoter, SV40 enhancer and an effector plasmid with the PSMA enhancer and promoter or Mk promoter to achieve novel tumor-specific transcriptional amplification for prostate cancer, and evaluated selectiveness to drive gene expression in LNCaP and PC-3 cancer cells. In PSMA-positive LNCaP cells and Mk-positive PC-3 cells, the TSTA system with each promoter and enhancer showed greater activity than one-step transcription with each promoter, as confirmed by growth inhibition of the cells and PC-3 tumor xenografts on suicide gene therapy.

Materials and Methods

Plasmid construction

pGL3-control, pGL3-enhancer and pGL3-basic plasmids were purchased from Promega (Madison, WI, USA). pFR-luc plasmid for expression of the luciferase gene controlled by a synthetic promoter that contains the yeast GAL4-binding sites in front of the E1B minimal promoter was obtained from Stratagene (La Jolla, CA, USA). The HSV-tk cDNA fragment was amplified as described previously.[22] This cDNA was then subcloned into the *Nco*I and *Xba*I restriction enzyme sites of the pGL3 enhancer vector, and pGL3-tk was constructed.

For amplification of the GAL4–VP16 fusion protein, the cDNA encoding the GAL4–VP16 fusion protein was generated as follows by site-directed mutagenesis by overlap extension using polymerase chain reaction (PCR).[23] The yeast GAL4 cDNA was amplified by PCR using the primer set GAL4-forward primer (FW), 5′-ATCCATGGaccATGAAGCTACTGTCTTCTAT-3′ and GAL4-reverse primer (RW), 5′-CGGTCGGGGG-GGCCGTCGAGACAGTCAACTGTCT-3′. The GAL4-FW contained a 3-bp optimal Kozak sequence (in lowercase letters) together with a *Nco*I restriction site (underlined). The GAL4-RW coded for the N-terminal region of the activation domain of VP16 (underlined), followed by the C-terminal region of GAL4. The cDNA coding for the activation domain of VP16 was amplified by PCR using the primer set VP16-FW, 5′-ACAGTTGACTGTATCGACGGCCCCCCCGACCGAT-3′ and VP16-RW, CATATAGACTATCCCGGACCCGGGGAA-TCC-3′. The forward primer, VP16-FW, coded for the C-terminal

doi: 10.1111/j.1349-7006.2006.00243.x

region of GAL4 (underlined), followed by the N-terminal region of the activation domain of VP16. The reverse primer, VP16-RW, coded for the VP16 sequence with an *Xba*I restriction site (underlined). The amplified PCR fragment of the GAL4–VP16 fusion protein by overlap extension (~0.6 kb in length) was subcloned into the *Nco*I and *Xba*I restriction enzyme sites of the pGL3 enhancer vector, and pGL3-GAL/VP was constructed.

For the construction of plasmids containing the PSMA promoter and enhancer, we cloned the DNA fragments by PCR amplification from normal human genomic DNA (Seegene, Seoul, Korea). The primer sets were determined according to the findings reported by Ikegami *et al.*,[17] and were PSMA(P)-FW, 5′-GAACTCGAGCCTACTCAGCTGGCCCA-3′ and PSMA(P)-RW, 5′-CTTAAGCTTGCTGCTGCTCTACTGCGCGC-3′ to amplify a DNA fragment for the PSMA promoter located between −1283 and −39. The forward and reverse primers, respectively, contained *Xho*I and *Hind*III restriction sites (underlined).

The PSMA enhancer fragment was cloned by nested-PCR amplification. The first PCR primer set was PSMA(E)1-FW, 5′-GGATGTGGCAAGTCGTAGTTGATTTGGT-3′, and PSMA(E)1-RW, 5′-GCTGTGTACCAATTGACAAGCAGT-GACA-3′. The nested-PCR primer set was PSMA(E)2-FW, 5′-GAAGGTACCCTTCTAAAATGAGTTGGG-3′, and PSMA(E)2-RW, 5′-GAACTCGAGGGCTACTACATAAG-TATAAGT-3′, to amplify the DNA fragment for the PSMA enhancer located between +11 958 and +13 606. The forward and reverse primers, respectively, contained *Kpn*I and *Xho*I restriction sites (underlined). The amplified PCR fragment of the PSMA promoter (~1.2 kb in length) was subcloned into the *Xho*I and *Hind*III restriction enzyme sites of the pGL3 enhancer, pGL3-tk and pGL3-GAL/VP vectors, and pPSMA(P)-luc, pPSMA(P)-tk and pPSMA(P)-GAL4-VP, respectively, were constructed. Subsequently, the amplified PCR fragment of the PSMA enhancer (~1.6 kb in length) was cloned into the *Kpn*I and *Xho*I restriction sites of the above plasmids, and pPSMA(EP)-luc, pPSMA(EP)-tk and pPSMA(EP)-GAL/VP, respectively, were constructed.

For the construction of plasmids containing the PSA promoter and enhancer, the primer sets were determined according to the findings of Pang *et al.*[24] One primer set was PSA(P)-FW, 5′-GAACTCGAGTTGGAATTCCACATTGTTG-3′ and PSA(P)-RW, 5′-GTTCCATGGTGACACAGCTCTC-CGGGTGC-3′ for the PSA promoter located between −636 and +46. The forward and reverse primers, respectively, contained *Xho*I and *Nco*I restriction sites (underlined). The other set was PSA(E)-FW, 5′-GAAGGTACCCTGCAGAGAAATTAATT-GTG-3′ and PSA(E)-RW, 5′-GAACTCGAGAATTCTCCAT-GGTTCTGTCA-3′ to amplify the DNA fragment for the PSA enhancer located between −4757 and −3928. The forward and reverse primers, respectively, contained *Kpn*I and *Xho*I restriction sites (underlined). The amplified PCR fragment of the PSA promoter (~0.6 kb in length) was subcloned into the *Xho*I and *Nco*I restriction sites of the pGL3 enhancer vector, and pPSA(P)-luc was constructed. Subsequently, the amplified PCR fragment of the PSA enhancer (~0.8 kb in length) was subcloned into the *Kpn*I and *Xho*I restriction sites of pPSA(P)-luc, and pPSA(EP)-luc was constructed.

For the construction of plasmids containing a Mk promoter, we designed a pair of primers incorporating artificially introduced restriction enzyme sites for PCR amplification according to findings reported previously.[13] The primer set was Mk(P)-FW, 5′-GAAGGTACCGCTTCCCTGCCCACCCGCGG-3′ and Mk(P)-RW, 5′-GTTCCATGGGCTTCGCTCCCTCCCGCGCC-3′ to amplify a DNA fragment for the Mk promoter stretching from bp −559 of the 5′ upstream flanking region to bp 27 of exon 1 of the human Mk gene. The forward and reverse primers, respectively, contained *Kpn*I and *Hind*III restriction sites (underlined). The amplified PCR fragment of the Mk promoter (~0.6 kb in length) was subcloned into the *Kpn*I and *Hind*III restriction sites of the pGL3 enhancer and pGL3-tk and pGL3-GAL/VP, and pMk(P)-luc, pMk(P)-tk and pMk(P)-GAL/VP, respectively, were constructed.

For the construction of reporter plasmids, the primer set was Syn-FW, 5′-CCAAGCTTGCATGCCTGCAG-3′ and Syn-RW, 5′-ATCCATGGTACCAACAGTACCGGAA-3′ to amplify a DNA fragment for a synthetic promoter that contained the yeast GAL4-binding site in front of the E1B minimal promoter of adenovirus. The forward and reverse primers, respectively, contained *Hind*III and *Nco*I restriction sites (underlined). The amplified PCR fragment of the synthetic promoter from pFR-luc (~0.2 kb in length) was subcloned into the *Hind*III and *Nco*I restriction sites of the pGL3 enhancer and pGL3-tk vector, and pRep-luc and pRep-tk, respectively, were constructed.

The plasmid pCMV-tk encoding HSV-tk under the control of the cytomegalovirus (CMV) promoter was constructed as described previously.[22] The plasmid pCMV-luc, encoding luciferase under the CMV promoter, was constructed by insertion of the CMV promoter into the pGL3 enhancer, as described previously.[22] A protein-free preparation of the plasmid was purified following alkaline lysis using maxiprep columns (Qiagen, Hilden, Germany).

Cell culture

LNCaP cells were supplied by the Department of Urology, Keio University Hospital (Tokyo, Japan). PC-3 cells were obtained from the Cell Resource Center for Biomedical Research, Tohoku University (Miyagi, Japan). Human cervix carcinoma HeLa cells were kindly provided by Toyobo (Osaka, Japan). All of the cell lines used in this study were grown in RPMI-1640 medium (Life Technologies, Grand Island, NY, USA) supplemented with 10% heat-inactivated fetal bovine serum (Life Technologies) and kanamycin (100 μg/mL) at 37°C in a humidified atmosphere with 5% CO_2.

RNA isolation and reverse transcription–polymerase chain reaction

Total RNA was isolated from LNCaP, PC-3 and HeLa cells, using NucleoSpin RNA II (Macherey-Nagel, Düren, Germany). Total RNA from normal and malignant prostate cells were purchased from Ambion (First Choice Tumor/Normal Adjacent Prostate Total RNA and First Choice Prostate Tumor Total RNA; Austin, TX, USA). First-strand cDNA was synthesized from 5 μg of total RNA as described previously.[22] Reverse transcription (RT)-PCR was carried out in a 25-μL reaction volume containing the following: 1 μL of synthesized cDNA, 10 pmol of each specific primer pair, and 0.25 units of Ex *Taq* DNA polymerase (Takara Shuzo, Kyoto, Japan) with a PCR buffer containing 1.5 mM $MgCl_2$ and 0.2 mM of each dNTP. The

profile of PCR amplification consisted of denaturation at 94°C for 0.5 min, primer annealing at 58°C for 0.5 min, and elongation at 72°C for 1 min for 25 cycles. PCR of the housekeeping gene β-actin, Mk and PSMA were carried out during the same cycle run for all samples. The PCR products for Mk, PSMA and β-actin were analyzed by 1.5% agarose gel electrophoresis in a Tris-Borate-ethylenediamine tetraacetic acid (TBE) buffer. The products were visualized by ethidium bromide staining.

Real-time PCR was carried out on the corresponding cDNA synthesized from each sample described above. The optimized settings were transferred to real-time PCR protocols on iCycler MyiQ detection systems (Bio-Rad Laboratories, Hercules, CA, USA) and SYBR Green I assay (iQ SYBER Green Supermix, Bio-Rad Laboratories) was used for quantification. Samples were run in triplicate and the expression level of Mk and PSMA mRNA was normalized for the amount of β-actin in the same sample. The difference of one cycle was calculated as a two-fold change in gene expression.

In vitro transfection

Cholesteryl-3β-carboxyamidoethylene-*N*-hydroxyethylamine (OH-Chol) was synthesized as reported previously.[25] The nanoparticle (NP) as a gene transfection reagent was prepared with lipids (OH-Chol : Tween 80 [NOF, Tokyo, Japan] 95 : 5, molar ratio = 10 : 1.3, weight) in 10 mL of water using a modified ethanol injection method as described previously.[22,25] Based on preliminary experiments with the cotransfected plasmids, the optimized ratio (w/w) of effector : reporter plasmid was determined as 1 : 1. The nanoplex at a charge ratio (+/–) of cationic lipid to DNA of 3/1 was formed by addition of NP to 2 μg of DNA (e.g. 1 μg of effector plasmid and 1 μg of reporter plasmid in the TSTA system) in 50 mM NaCl with gentle shaking and left at room temperature for 10 min. For transfection, the nanoplex was diluted in 1 mL of medium supplemented with 10% serum and then incubated for 24 h. Androgen stimulation of transfected cells was carried out by adding 10 nM dihydrotestosterone (DHT; Sigma, St Louis, MO, USA) to the culture medium.

Luciferase assay

Cell cultures were prepared by plating cells in a 35-mm culture dish 24 h prior to each experiment. The cells at 70% confluence were transfected as described above. Luciferase expression was measured as counts per s (cps)/μg protein using the luciferase assay system (Pica gene; Toyo Ink Manufacturing, Tokyo, Japan) and bicinchoninic acid (BCA) reagent (Pierce, Rockford, IL, USA) as reported previously.[22]

In vitro sensitivity to the ganciclovir assay

LNCaP, PC-3 and HeLa cells were seeded separately at a density of 1×10^4 cells per well in 96-well plates and maintained for 12 h before transfection in RPMI-1640 medium supplemented with 10% serum. The cells were transfected with the nanoplexes at 0.2 μg plasmid/well. After 12 h incubation, the culture medium was replaced with medium containing various concentrations of ganciclovir (GCV; Glaxo Smith Kline, Helis, UK) ranging from 0.1 to 1000 μg/mL. The number of surviving cells was determined with a WST-8 assay (Dojindo Laboratories, Kumamoto, Japan) after 3 days' exposure to GCV as described previously.[22]

Immunoblotting

LNCaP, PC-3 and HeLa cells were transfected with various plasmids and then incubated for 24 h. The cells were suspended in lysis buffer (0.5% Triton-X 100 in phosphate-buffered saline pH 7.4), then centrifuged at 15 000 r.p.m. (20 000 × g) for 10 min. The supernatants were resolved by 12% sodium dodecyl sulfate–polyacrylamide gel electrophoresis and transferred to a polyvinylidene difluoride (PVDF) membrane (FluoroTrans W; PALL Gelman Laboratory, Ann Arbor, MI, USA). HSV-tk was identified using a specific rabbit antiserum (kindly provided by the Department of Virology, Toyama Medical and Pharmaceutical University) with antirabbit IgG peroxidase conjugate (Santa Cruz Biotechnology, Santa Cruz, CA, USA) as the secondary antibody and detected with peroxidase-induced chemiluminescence (Super Signal West Pico Chemiluminescent Substrate; Pierce).

Assessment of PC-3 xenograft tumor growth *in vivo*

To generate PC-3 tumor xenografts, 1×10^7 cells suspended in 50 μL of RPMI-1640 medium containing 60% reconstituted basement membrane (Matrigel; Collaborative Research, Bedford, MA, USA) were inoculated subcutaneously into the flanking region of male BALB/c nu/nμ mice (6 weeks of age; CLEA Japan, Tokyo, Japan). The tumor volume was calculated using the formula:

$$\text{tumor volume} = 0.5ab^2,$$

where a and b are the larger and smaller diameters, respectively. When the average volume of PC-3 xenograft tumors reached 150 mm^3 (day 0), these mice were divided into four groups: group I, pGL3-basic (10 μg) as a control; group II, pMk(P)-tk (10 μg); group III, pMk(P)-GAL/VP (5 μg) plus pRep-tk (5 μg); and group IV, pCMV-tk (10 μg) Each experimental group consisted of four tumors. Based on a preliminary experiment of gene expression by intratumoral injection, the optimized ratio of cationic lipid to DNA was determined as 1 : 1. The nanoplex at a charge ratio (+/–) of 1/1 of cationic lipid to DNA was formed by addition of NP (15.8 μL) to 10 μg of DNA with gentle shaking and incubation at room temperature for 10 min. The nanoplexes of 10 μg of plasmid per tumor were injected directly into xenografts on days 0, 3 and 6. GCV at a dose of 25 mg/kg was administered intraperitoneally 12, 24 and 36 h after the injections of nanoplexes. The tumor volume was measured at days 0, 3, 6, 8, 10, 12 and 14.

Statistical analysis

The statistical significance of differences between mean values was determined using Welch's *t*-test. Multiple measurement comparisons were carried out by analysis of variance followed by the Bonferroni/Dunn test. For the animal study, statistical comparisons were carried out using Fisher's exact test. *P*-values less than 0.05 were considered significant.

Results

Expression of midkine and PSMA mRNA

First, we investigated the expression of Mk and PSMA in human prostate malignant biopsy and LNCaP, PC-3 and HeLa cells using the quantitative PCR and RT-PCR method (Fig. 2). HeLa cells were used as a Mk-positive control.[26] In

doi: 10.1111/j.1349-7006.2006.00243.x

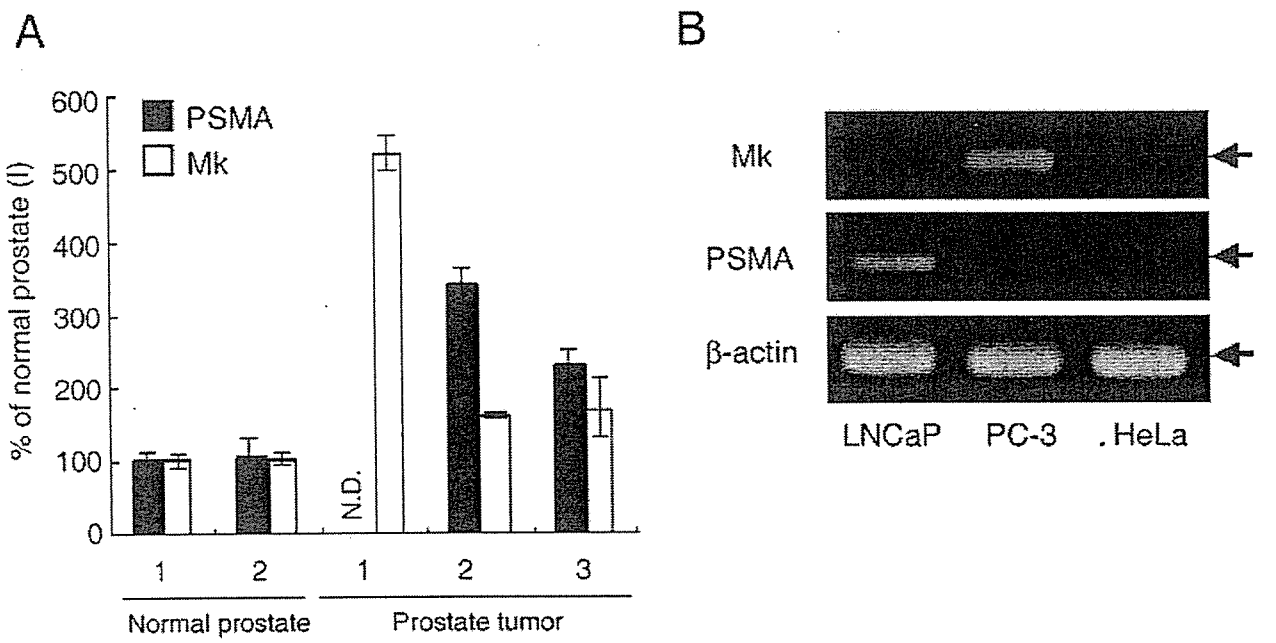

Fig. 2. (A) Relative amount of midkine (Mk) and prostate-specific membrane antigen (PSMA) mRNA in normal and malignant prostate was compared by SYBR Green I-based quantitative polymerase chain reaction analysis. The *y*-axis indicated the fold induction of gene expression. The expression level of Mk and PSMA mRNA was normalized for the amount of β-actin in the same sample. Each result represents the mean ± SD ($n = 3$). (B) Expression of Mk and PSMA mRNA in LNCaP, PC-3 and HeLa cells detected by reverse transcription–polymerase chain reaction.

the human prostate biopsy, two kinds of RNA from normal prostate and three prostate tumors were used. Elevated expression of PSMA and/or Mk mRNA was observed in prostate tumor (Fig. 2A), indicating that upregulated expression of PSMA and Mk could be utilized as a marker for prostate tumor. Mk mRNA was expressed strongly in PC-3 cells and weakly in HeLa cells, but was not detected in LNCaP cells (Fig. 2B). Quantitative PCR analysis showed that the amount of Mk mRNA in PC-3 cells was 31-fold higher than in HeLa cells (data not shown). PSMA mRNA was detected in LNCaP cells, but not in PC-3 or HeLa cells. This result suggested that PC-3 and HeLa cells could be utilized with the Mk promoter for tumor-specific expression, and LNCaP cells could be utilized with the PSMA promoter.

Analysis of PSMA and PSA enhancer/promoter activity

In a preliminary study, we evaluated the activities of the PSA and PSMA promoters as they have been well characterized and determined to be tissue specific. PSMA promoter activity was increased with a combination of SV40 enhancer in LNCaP cells.[27] Therefore, we used the combination of PSA or PSMA enhancer and promoter and SV40 enhancer to enhance prostate-specific gene expression (Fig. 1). To assess the transcriptional activity of our cloned promoter and enhancer regions, we constructed two PSA promoter-based plasmids, pPSA(P)-luc and pPSA(EP)-luc coding for the luciferase gene under the control of the PSA promoter and PSA enhancer and promoter, respectively, and two PSMA promoter-based plasmids, pPSMA(P)-luc and pPSMA-(EP)-luc coding for the luciferase gene under the control of the PSMA promoter and PSMA enhancer and promoter, respectively (Table 1). Four kinds of plasmids (2 μg) were transfected into LNCaP cells cultured in the absence or presence of DHT or into PC-3 cells, and a luciferase assay was carried out 24 h after transfection. We normalized each experiment using SV40 constructs (pGL3-control) (Fig. 3). It has been reported that LNCaP cells are androgen responsive, showing a decrease in PSMA mRNA levels and increase in PSA mRNA levels with increasing androgen concentrations in culture media.[28–30] In the medium without DHT, PSA-related plasmids, pPSA(P)-luc and pPSA(EP)-luc, exhibited weak transfectional activity (11 and 24% of the luciferase activity with pGL3-control) in LNCaP cells. However, in the medium with DHT, pPSA(EP)-luc, but not pPSA(P)-luc, increased the luciferase activity 6.3-fold compared to that in medium without DHT (151% of pGL3-control). Among the PSMA promoter-based plasmids, pPSMA(P)-luc showed weak transfection activity (28.8% and 45.9% of pGL3-control in medium without or with DHT, respectively). In contrast, pPSMA(EP)-luc induced relatively strong transfection activity (153% of pGL3-control) in medium without DHT and a small decrease of 36% in medium with DHT in LNCaP cells. In PC-3 cells, pPSA(P)-luc, pPSA(EP)-luc, pPSMA(P)-luc and pPSMA(EP)-luc drove only 2.3%, 13.1%, 17.8% and 22.5%, respectively, of the luciferase activity of pGL3-control. We confirmed that our cloned promoter and enhancer regions of PSA and PSMA had prostate-specific transcriptional activity consistent with findings reported previously.[28,29,31,32]

Two-step transcriptional amplification system using the PSMA promoter

The PSMA promoter appeared to be suitable for gene therapy because the expression of PSMA was not strongly affected

Table 1. Plasmids used in this study

Transcription		Plasmid	Upstream of expression gene		Expression gene
			Enhancer	Promoter	
One-step		pGL3-control	–	SV40	Luciferase
		pCMV-luc	CMV	CMV	Luciferase
		pCMV-tk	CMV	CMV	HSV-tk
		pPSA(P)-luc	–	PSA (0.6 kb)	Luciferase
		pPSA(EP)-luc	PSA (0.8 kb)	PSA (0.6 kb)	Luciferase
		pPSMA(P)-luc	–	PSMA (1.2 kb)	Luciferase
		pPSMA(EP)-luc	PSMA (1.6 kb)	PSMA (1.2 kb)	Luciferase
		pPSMA(EP)-tk	PSMA (1.6 kb)	PSMA (1.2 kb)	HSV-tk
		pMk(P)-luc	–	Midkine (0.6 kb)	Luciferase
		pMk(P)-tk	–	Midkine (0.6 kb)	HSV-tk
Two-step	Effector	pPSMA(EP)-GAL/VP	PSMA (1.6 kb)	PSMA (1.2 kb)	GAL4/VP16
	Plasmid	pMk(P)-GAL/VP	–	Midkine (0.6 kb)	GAL4/VP16
	Reporter	pRep-luc	–	5 × GAL4 bs + Minimal	Luciferase
	Plasmid	pRep-tk	–	5 × GAL4 bs + Minimal	HSV-tk

All plasmids contained SV40 enhancer in downstream of expression gene. GAL4 bs, GAL4 binding site; HSV-tk, herpes simplex virus thymidine kinase; minimal, adenoviral E1B minimal promoter; Mk(P), midkine promoter; PSA, prostate-specific antigen; PSA(EP), PSA enhancer and promoter; PSA(P), PSA promoter; PSMA, prostate-specific membrane antigen; PSMA(EP), PSMA enhancer and promoter; PSMA(P), PSMA promoter.

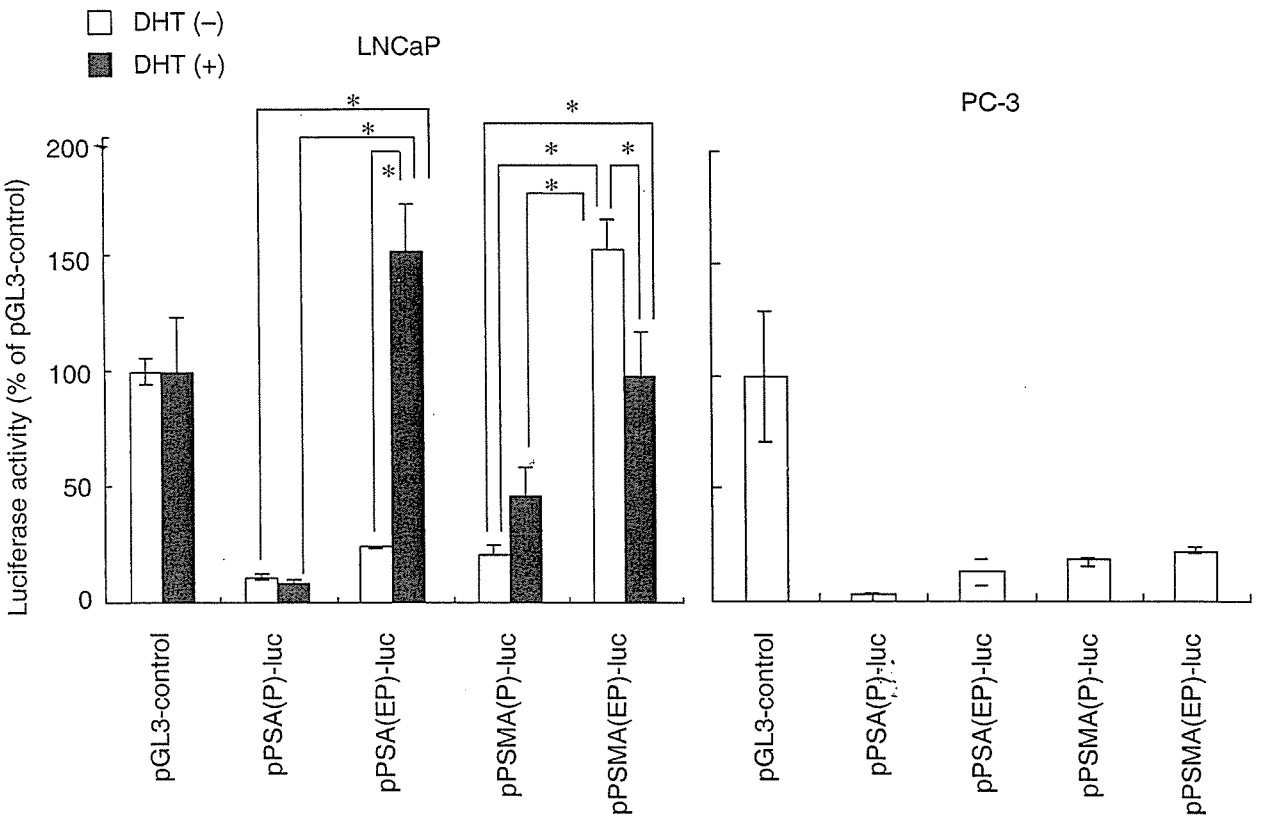

Fig. 3. Prostate-specific antigen (PSA) or prostate-specific membrane antigen (PSMA) enhancer and promoter activities in the absence or presence of dihydrotestosterone (DHT) in LNCaP and PC-3 cells. The prostate cancer cell lines, PSA-positive and PSMA-positive LNCaP cells and PSA-negative and PSMA-negative PC-3 cells were transfected with the plasmids indicated (2 μg). The promoter and enhancer activities were determined with a luciferase expression assay: 100% luciferase activity was taken as that of the pGL3-control. The results were expressed as the mean ± SD ($n = 4$). Statistical significance of the data was evaluated using the Bonferroni/Dunn test. *$P < 0.05$.

by the presence or absence of androgen. However, the PSMA enhancer and promoter do not have strong promoter activity even when combined with the SV40 enhancer. Therefore, to enhance the PSMA promoter activity, we constructed the PSMA promoter-based effector plasmid pPSMA(EP)-GAL/VP coding for the GAL4–VP16 fusion protein under control of the PSMA enhancer and promoter, and a reporter plasmid, pRep-luc, coding for a luciferase gene under the control of a

doi: 10.1111/j.1349-7006.2006.00243.x

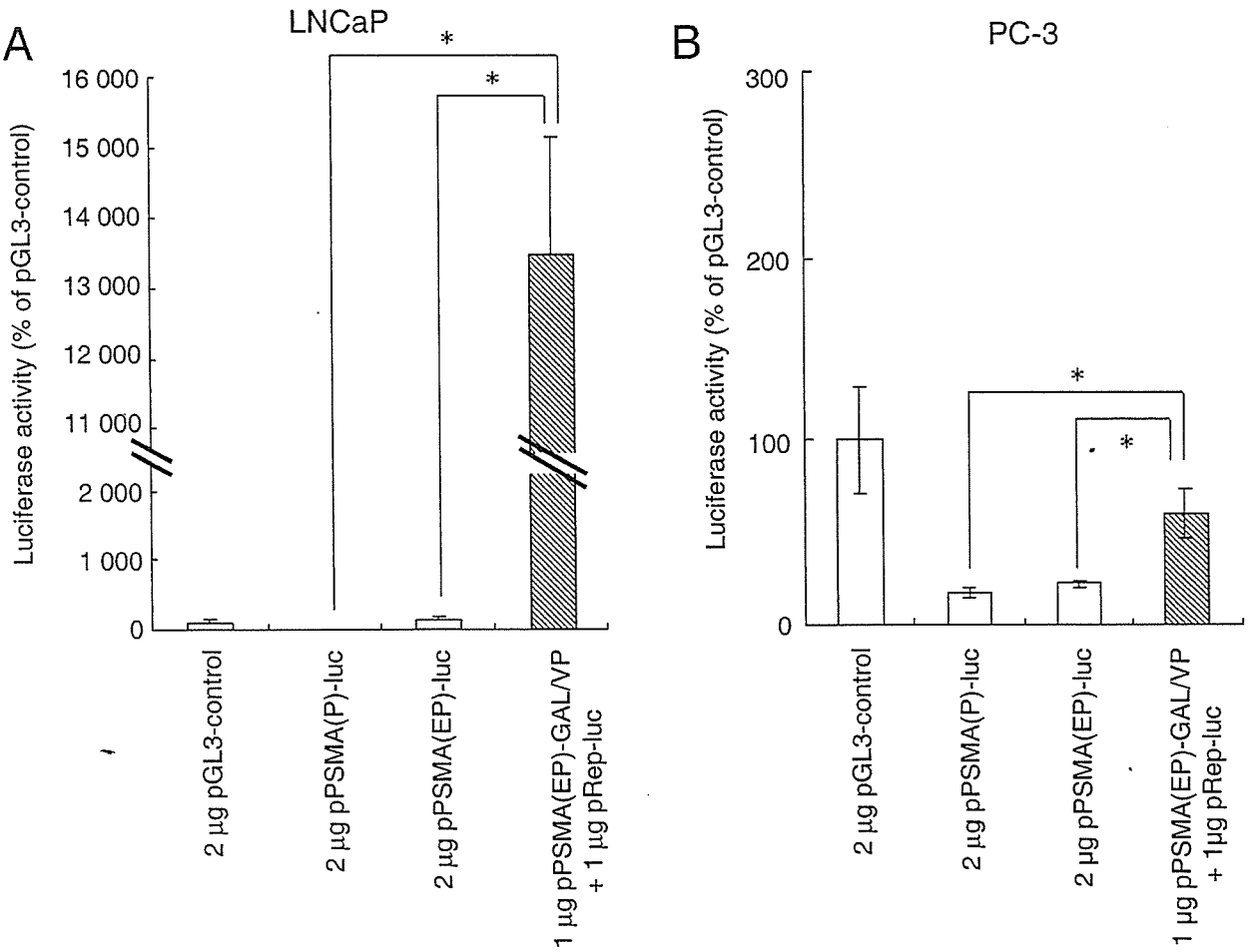

Fig. 4. Enhancement of the prostate-specific membrane antigen (PSMA) promoter activities by the two-step transcriptional amplification (TSTA) system determined using a luciferase expression assay in (A) LNCaP and (B) PC-3 cells. Comparison of transcriptional activity between one-step transcription (pPSMA[P]-luc or pPSMA[EP]-luc) and the TSTA system (pPSMA[EP]-GAL/VP plus pRep-luc). The luciferase activity of pGL3-control is taken as 100%. The results were expressed as the mean ($n = 4$). Statistical significance of the data was evaluated using the Bonferroni/Dunn test. *$P < 0.05$.

synthetic promoter composed of 5 × GAL4-binding sites and the adenoviral E1B minimal promoter with the SV40 enhancer (Table 1), and evaluated luciferase activity by conducting cotransfection assays in LNCaP and PC-3 cells.

Strong luciferase activity was observed when the combination of pPSMA(EP)-GAL/VP and pRep-luc was transfected into LNCaP cells (Fig. 4A), but not when either pPSMA(EP)-GAL/VP or pRep-luc alone was transfected into the cell lines (1.7% and 3.8% of pGL3-control, respectively; data not shown). The paired plasmid, pPSMA(EP)-GAL/VP and pRep-luc (13 500% of pGL3-control, equivalent to approximately 45 000 cps/μg protein) showed 85-fold and 640-fold more luciferase activity than pPSMA(EP)-luc and pPSMA(P)-luc, respectively, in LNCaP cells (Fig. 4A), but showed comparatively less promoter activity, approximately 61% of pGL3-control in PC-3 cells (Fig. 4B). Luciferase activity by the paired plasmid, pPSMA(EP)-GAL/VP and pRep-luc, in LNCaP cells was 2.7% of that by CMV promoter (data not shown). This suggested that the TSTA system induced strong activity in PSMA-positive LNCaP cells but comparatively less activity in PC-3 cells.

Two-step transcriptional amplification system using the Mk promoter

To examine the TSTA system using another promoter, we constructed Mk promoter-based plasmids, pMk(P)-luc and pMk(P)-GAL/VP coding for the luciferase gene and GAL4–VP16 fusion protein, respectively, under control of the Mk promoter and SV40 enhancer (Table 1). We cloned a DNA fragment for the Mk promoter stretching from bp 27 of exon 1 to bp 559 of the 5′ flanking region of the human Mk gene. The 2.3-kb genomic fragment in the 5′ region of the Mk gene contained the elements responsible for promoter activity.[33] The Mk enhancer is composed of two elements, which are located between bp −1006 and −895 and between bp −901 and −794.[34] However, Yoshida *et al.* reported that the transcriptional activity mediated by a fragment spanning bp −559 to +50 was stronger than that mediated by a fragment stretching from bp −2285 to 50.[13] Therefore, this fragment would be suitable for the Mk promoter. In Mk-positive PC-3 and HeLa cells, the paired plasmid, pMk(P)-GAL/VP and pRep-luc, showed 5.0-fold and 2.6-fold higher luciferase

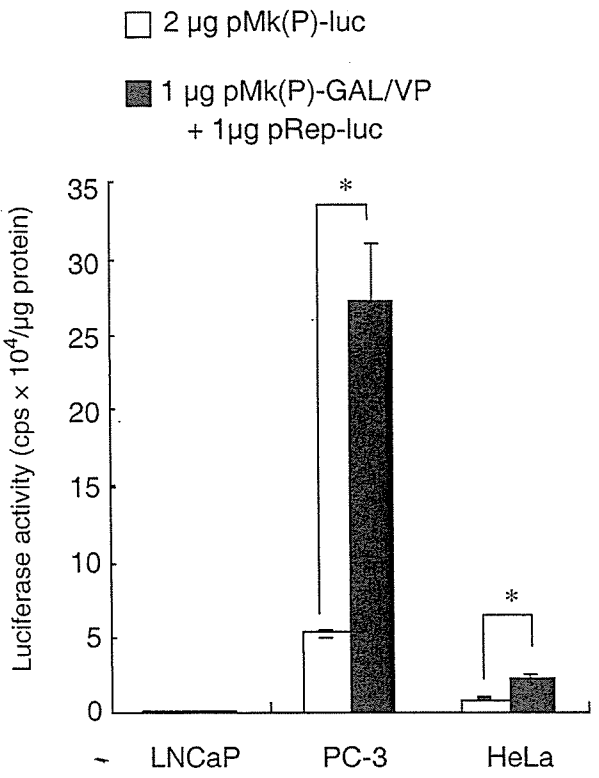

Fig. 5. Enhancement of the midkine (Mk) promoter activities by the two-step transcriptional amplification (TSTA) system determined using a luciferase expression assay among LNCaP, PC-3 and HeLa cells. Comparisonal of transcriptional activities of the Mk promoter among cell lines using one-step transcription (pMk[P]-luc) and the TSTA system (pMk[P]-GAL/VP and pRep-luc). The luciferase activity was expressed as counts per s (cps)/μg protein. The results were expressed as the mean ± SD ($n = 4$). Statistical significance of the data was evaluated using the Welch's t-test. *$P < 0.05$, compared with pMk(P)-luc.

activities, respectively (270 000 and 22 400 cps/μg protein, equivalent to approximately 9100% and 5500% of the pGL3-control), than the plasmid pMk(P)-luc (54 000 and 8500 cps/μg protein, equivalent to approximately 1800% and 2100% of the pGL3-control) (Fig. 5). Luciferase activities by the paired plasmid, pMk(P)-GAL/VP and pRep-luc, in PC-3 and HeLa cells were 22.1% and 3.7%, respectively, of that by the CMV promoter, (data not shown). However, strong luciferase activity was not observed when either pMk(P)-GAL/VP (0.1% and 4.2% of pGL3-control in PC-3 and HeLa cells, respectively) or pRep-luc alone (8.1% and 11.1% of pGL3-control, respectively) was transfected into the cells (data not shown). The paired plasmids did not induce luciferase activity in LNCaP cells (Fig. 5), suggesting that the TSTA system with the Mk promoter did not induce promoter activity in Mk-negative LNCaP cells.

In vitro suicide gene therapy model in PSMA-positive LNCaP cells and Mk-positive PC-3 and HeLa cells

Next, we applied the TSTA system to suicide gene therapy with the HSV-tk gene. pPSMA(EP)-tk or a paired plasmid, pPSMA(EP)-GAL/VP and pRep-tk, was transfected into LNCaP and PC-3 cells, and the inhibitory effect on cell growth was investigated in the presence of various concentrations of GCV. pCMV-tk and pGL3-basic were used as positive and negative controls, respectively. In LNCaP cells, the paired plasmids significantly inhibited cell growth (Fig. 6A). However, pPSMA(EP)-tk did not inhibit cell growth, having a similar effect to pGL3-basic. The therapeutic effects were also tested in PSMA-negative PC-3 cells, and the paired plasmids showed no inhibitory effect (Fig. 6B). pCMV-tk exerted inhibitory effects on LNCaP and PC-3 cells (Fig. 6A,B). These results indicated that a combination of pPSMA(EP)-GAL/VP and pRep-tk would be better for gene therapy against PSMA-positive cells.

In PC-3 and HeLa cells, the paired plasmids pMk(P)-GAL/VP and pRep-tk showed significant inhibitory effects, but pMk(P)-tk did not (Fig. 7A,B). The paired plasmids showed very similar inhibition to pCMV-tk in PC-3 and HeLa cells. In Mk-negative LNCaP cells, the paired plasmids did not actually inhibit cell growth (Fig. 7C). It appears that a combination of pMk(P)-GAL/VP and pRep-tk would be better for gene therapy against Mk-positive cells.

Western blot analysis

We investigated whether the observed inhibitory effects in the TSTA system with the Mk promoter corresponded with the expression level of HSV-tk protein (Fig. 7D). HSV-tk expression on transfection of pCMV-tk was observed clearly in all cell lines. The paired plasmids pMk(P)-GAL/VP and pRep-tk more markedly expressed HSV-tk than pMk(P)-tk in PC-3 and HeLa cells. In PC-3 cells, the paired plasmid showed a similar expression level to pCMV-tk. In Mk-negative LNCaP cells, pMk(P)-tk and the paired plasmids did not induce HSV-tk expression.

In vivo suicide gene therapy in PC-3 tumor xenografts

The TSTA system with the Mk promoter in PC-3 cells (22% of CMV promoter) induced stronger luciferase activity than that with the PSMA promoter in LNCaP cells (2.7% of CMV promoter). Therefore, we evaluated the antitumor effect by direct injection of the nanoplexes into PC-3 tumor xenografts. The average growth rate of tumors was suppressed significantly in the mice treated with the nanoplex of the paired plasmid, pMk(P)-GAL/VP and pRep-tk, compared with the control mice (Fig. 8). The paired plasmid showed similar growth inhibition to pCMV-tk. These results indicated that the TSTA system with the Mk promoter could induce greater inhibition of tumor growth than one-step transcription with the Mk promoter.

Discussion

The activity of a prostate tumor-specific promoter is generally weak in comparison to that of a universal promoter such as the CMV promoter.[14,35] Therefore, in the present study, a TSTA system was used to enhance the efficacy of suicide gene therapy for treatment of prostate tumor. The TSTA systems showed greater activity than one-step transcription, as confirmed by the growth inhibition of PSMA-positive LNCaP cells and Mk-positive PC-3 cells, and PC-3 tumor xenografts on suicide gene therapy. This suggests that TSTA systems featuring tumor-specific promoters are suitable for cancer treatment by gene therapy.

doi: 10.1111/j.1349-7006.2006.00243.x